ARTICLE

MYC upstream region orchestrates resistance to PI3K inhibitors in cancer cells through FOXO3a-mediated autophagic adaptation

Rosa Bordone[1,7], Devon Michael Ivy[1,7], Rodrigo D'Amico[1], Martina Barba[1], Miriam Gaggianesi[2], Fiorella Di Pastena[3], Bianca Cesaro[4], Francesca Bufalieri[1], Alessio Balzerano[1], Enrico De Smaele[5], Giuseppe Giannini[1], Lucia Di Marcotullio[1], Alessandro Fatica[4], Giorgio Stassi[2], Laura Di Magno[1], Sonia Coni[1] and Gianluca Canettieri[1,6]✉

The MYC oncogene is frequently overexpressed in tumors and inhibition of its translation is considered an attractive therapeutic opportunity. Despite numerous reports proposing an internal ribosome entry site (IRES) within the MYC Upstream Region (MYC UR) to sustain MYC translation during cellular stress or chemotherapy, conflicting evidence remains regarding the validity of such a mechanism. Through comprehensive investigations in MYC-driven Colorectal Cancer (CRC) and Burkitt Lymphoma (BL) cells, we demonstrate that MYC UR does not facilitate cap-independent translation, but instead orchestrates resistance to PI3K inhibitors. Genomic deletion of MYC UR neither impacts MYC protein levels nor viability in CRC cells, either untreated or exposed to cellular stress. However, in response to PI3K inhibitors, MYC UR drives a FOXO3a-dependent transcriptional upregulation of MYC, conferring drug resistance. This resistance is mediated by enhanced autophagic flux, governed by MYC, and blockade of autophagy sensitizes CRC cells to PI3K inhibition in vitro and in vivo. Remarkably, BL cells lacking the translocation of MYC UR exhibit sensitivity to PI3K inhibitors, whereas MYC UR-translocated cells respond to these drugs only when autophagy is inhibited. These findings challenge previous notions regarding IRES-mediated translation and highlight a promising strategy to overcome resistance to PI3K inhibitors in MYC-driven malignancies, offering potential clinical implications for CRC and BL treatment.

Oncogene; https://doi.org/10.1038/s41388-024-03170-6

Graphical Abstract
In response to BKM120, the upstream region of MYC (UR) enhances MYC expression, via FOXO3a, leading to increased autophagic flux and resistance to PI3K inhibitors (left). Pharmacological blockade of autophagy (center) or lack of translocated MYC UR along with MYC CDS in BL (right) overcome resistance and induces cells death. Image created in BioRender.

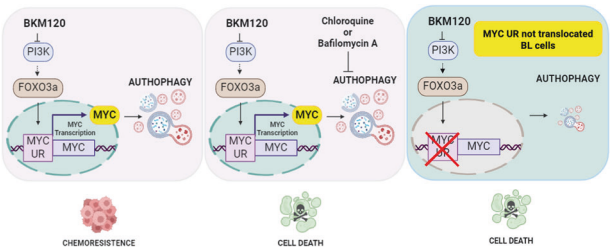

INTRODUCTION

The proto-oncogene MYC regulates key biological processes, such as proliferation, differentiation, translation, DNA repair, viability, and metabolism, by affecting transcription of nearly 15% of the genome in humans [1].

MYC was recognized as an oncogene when it was discovered to directly cause Burkitt Lymphoma (BL), a cancer characterized by chromosomal translocation of regions of the MYC gene and altered gene expression [2–5]. Since then, MYC dysregulation and/or abnormal expression [6] has been observed in more than 70%

[1]Department of Molecular Medicine, Sapienza University of Rome, Viale Regina Elena 291, 00161 Rome, Italy. [2]Department of Surgical, Oncological and Stomatological Sciences, University of Palermo, Via Liborio Giuffrè 5, 90127 Palermo, Italy. [3]McMaster University, Faculty of Health Sciences, Department of Medicine, 1200Main St W, Hamilton, ON, Canada. [4]Department of Biology and Biotechnologies "Charles Darwin", Sapienza University of Rome, Piazzale Aldo Moro 5, 00185 Rome, Italy. [5]Department of Experimental Medicine, Sapienza University of Rome, Viale Regina Elena 324, 00161 Rome, Italy. [6]Istituto Pasteur, Fondazione Cenci-Bolognetti, Sapienza University of Rome, Viale Regina Elena 291, 00161 Rome, Italy. [7]These authors contributed equally: Rosa Bordone, Devon Michael Ivy. ✉email: gianluca.canettieri@uniroma1.it

Received: 12 March 2024 Revised: 12 September 2024 Accepted: 13 September 2024
Published online: 22 September 2024

of human cancers, and in the majority of colorectal cancers (CRC), which are a major cause of human cancer mortality [7–10]. Aberrantly activated MYC confers selective growth advantage to cancer cells by rewiring their transcriptional programs and signaling modules [11]. For this reason, MYC is commonly considered on the top of the suitable targets in cancer therapy and many efforts are devoted to the identification of strategies that limit its aberrant expression and regulation. Because of the lack of druggable pockets and clefts, direct targeting of MYC with structure-based molecules seems not realistic, while alternative strategies, based on molecules affecting its dimerization properties or the intracellular content, are believed to have more chances

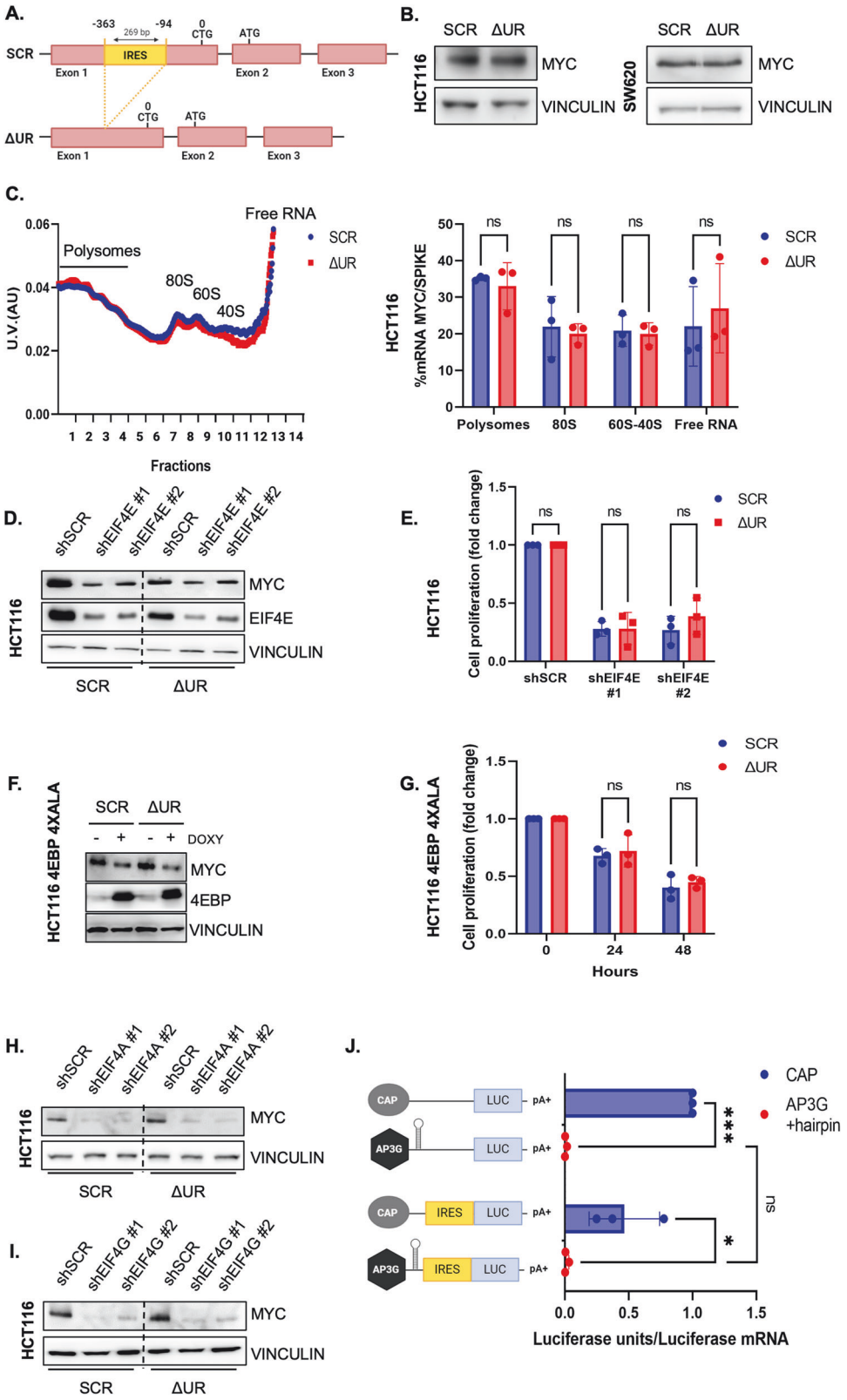

Fig. 1 The MYC UR does not mediate IRES-dependent translation in colon cancer cells. A Schematic representation of MYC IRES deletion using a CRISPR/Cas9 approach to generate UR-deleted (ΔUR) monoclonal cell lines and control cell lines (SCR). Image created in BioRender. **B** Immunoblot showing MYC protein levels in CRC ΔUR cells compared to SCR in both HCT116 (left panel) and SW620 (right panel). Vinculin is a loading control. **C** Polysome profile comparing global translation in HCT116 SCR and ΔUR cells. Left panel: The graph shows mean ultraviolet (UV) absorbance at 260 nm from 3 independent experiments of cytoplasmic lysates fractionated on 15–50% sucrose gradients. Right panel: QPCR analysis of MYC mRNA in the polysome fractions. A synthetic spike-in RNA was added to each fraction before RNA extraction and used as loading control (n = 3). **D** Immunoblot of MYC protein levels in SCR and ΔUR HCT116 cells after lentiviral-mediated knockdown of eIF4E using two different short hairpin RNAs for 72 h. **E** Proliferation assay of HCT116 SCR and ΔUR cells transduced with lentiviruses expressing two different shRNAs against eIF4E for 72 h, then reseeded and counted 48 h later. Cell proliferation is represented as the fold change compared to control (shSCR) cells (n = 3). **F** Immunoblot documenting MYC and 4EBP protein levels in SW620 cells infected with the lentivirus expressing doxycycline-inducible 4EBP mutated in the four phosphorylatable residues (4EBP 4XALA). Cells were treated with 1 μg/mL doxycycline for 72 h. **G** Proliferation assay of HCT116 SCR and ΔUR cells infected with 4EBP 4XALA lentivirus, selected with puromycin for 72 h then reseeded and treated with 1 μg/mL doxycycline. Cells were counted at the indicated time points. Cell proliferation is represented as the fold change compared to the corresponding untreated cells (n = 3). **H** Immunoblot showing MYC protein levels in HCT116 SCR and ΔUR cells 72 h post-infection with lentivirus expressing two different eIF4A-targeting shRNAs. **I** Immunoblot showing MYC protein levels in HCT116 SCR and ΔUR cells 72 h post-infection with lentivirus expressing two different eIF4G-targeting shRNAs. **J** Left panel: Schematic representation of in vitro transcribed (IVT) mRNA of the firefly luciferase reporter, cloned in the pSP64polyA plasmid with and without both the MYC IRES and a stable hairpin to block ribosome scanning. During the synthesis, 7-methylguanosine (CAP) or a non-functional CAP analog (AP3G) was added. Right panel: Luciferase assay after transfection of the in vitro transcribed RNA in SW620 cells for 6 h. Data were normalized by QPCR of luciferase mRNA and are expressed as fold change relative to cap-conjugated mRNAs (n = 3). Left panel created in BioRender. Data represent the mean ± SD of at least three experiments, each performed in triplicate. ns=not significant ($p > 0.05$), *$p < 0.05$, **$p < 0.01$, ****$p < 0.000,1$ by Two-way ANOVA followed by post-hoc Tukey's multivariate analysis.

of success [11, 12]. Among them, inhibition of MYC biosynthesis has emerged as a potentially valuable approach, and drugs inhibiting MYC translation have been tested in preclinical and clinical settings, providing promising results [13, 14].

MYC translation is initiated mostly through a canonical cap-dependent mechanism, triggered by the interaction of eIF4E with the cap structure of MYC mRNA [15]. However, drugs inhibiting cap-mediated initiation, such as mTOR inhibitors or some cellular stressors, fail to prevent MYC biosynthesis [16]. To explain this phenomenon, it was proposed that under these conditions MYC translation may be mediated by cap-independent mechanisms due to the presence of an internal ribosome entry site (IRES) in its 5′ UTR, which ranges specifically from 363 to 94 bases upstream its non-canonical CUG start codon [17, 18].

IRES-dependent translation was first discovered in the context of picornaviruses [19–21] which can initiate protein biosynthesis when canonical translation is blocked by the infection itself. In the past years, several authors identified putative IRES sequences in the 5′ untranslated regions of mammalian messenger RNAs, particularly in genes involved in cell viability, proliferation, and cell cycle regulation [22], such as MYC. It was hypothesized that IRES-dependent translation represents a salvage mechanism used by tumor cells to escape death and survive to different forms of cellular stress occurring in the tumor microenvironment, such as endoplasmic reticulum (ER), genotoxic, metabolic, and redox stresses [23–25]. Contrary to the viral counterpart, however, the function and relevance of cellular IRES has been questioned, largely because in most cases it was validated using reporter constructs [20] expressing single bicistronic transcripts, consisting of two reporter cistrons (e.g. renilla and firefly luciferase as in the pR-F plasmid) with the putative IRES placed in the intercistronic region [26]. In this system, the first cistron is translated through a canonical cap-mediated mechanism, while the second cistron is translated only if the intercistronic region allows internal entry of ribosomes [21].

Various researchers have demonstrated problems that can result from this approach [27–29]. For example, the pR-F plasmid has been shown to translate from the second cistron due to a cryptic promoter rather than from internal ribosome entry [27, 30, 31]. Other researchers have shown reporter translation occurring due to cryptic splicing that results in monocistronic luciferase transcripts [32].

Therefore, additional studies seem to be required to make the conclusion that certain untranslated regions may function as mediators of internal initiation.

As for the MYC oncogene, several reports have proposed that its IRES-dependent translation represents a central mechanism used by tumor cells to escape death and survive the unfavorable tumoral microenvironment in response to ER stress [33], genotoxic stress [23], or mTOR blockade [16]. Hence, MYC IRES has been suggested as a relevant actionable mechanism; the inhibition of which might prevent cancer cell survival under adverse conditions and resistance to chemotherapies.

However, as with the other cellular IRESes, the above-described studies were largely conducted using bicistronic reporter systems. Therefore, whether the IRES region of MYC promotes internal initiation under critical conditions and plays a relevant biological role in cancer still represents an open issue.

In the present work, we have sought to unequivocally resolve these controversies using comprehensive in vitro and in vivo approaches.

Our data presented here suggest that the endogenous upstream region (UR) of MYC is not used for internal ribosome initiation, but it rather functions as a transcriptional inducer of MYC in response to PI3K inhibition, leading to increased autophagic flux and drug resistance.

RESULTS

Deletion of the region corresponding to MYC IRES does not change MYC content and cell viability in CRC cells

We excised the region between 363 and 94 bases upstream the first start codon, previously identified as MYC IRES [17] (Fig. 1A and Supplementary Fig. 1A). We used HCT116 and SW620 CRC cells, where MYC IRES activity was previously reported [34, 35] and generated for each of them two gene-edited clones that we will refer to as ΔUR and SCR (scrambled control).

MYC protein and mRNA levels (Fig. 1B and Supplementary Fig. 1B) were not changed between ΔUR and SCR, suggesting that this region does not affect MYC content under standard culturing conditions. Subsequently, we performed polysomal fractionation to investigate whether deletion of the IRES region would affect the association of MYC mRNA to ribosomes. We did not observe changes of MYC mRNA distribution in cells deleted of the IRES region compared to SCR cells (Fig. 1C), suggesting that the IRES region does not contribute to initiation of MYC translation in this setting.

To further investigate this aspect, we examined the effect of inactivation of key regulators of translational initiation.

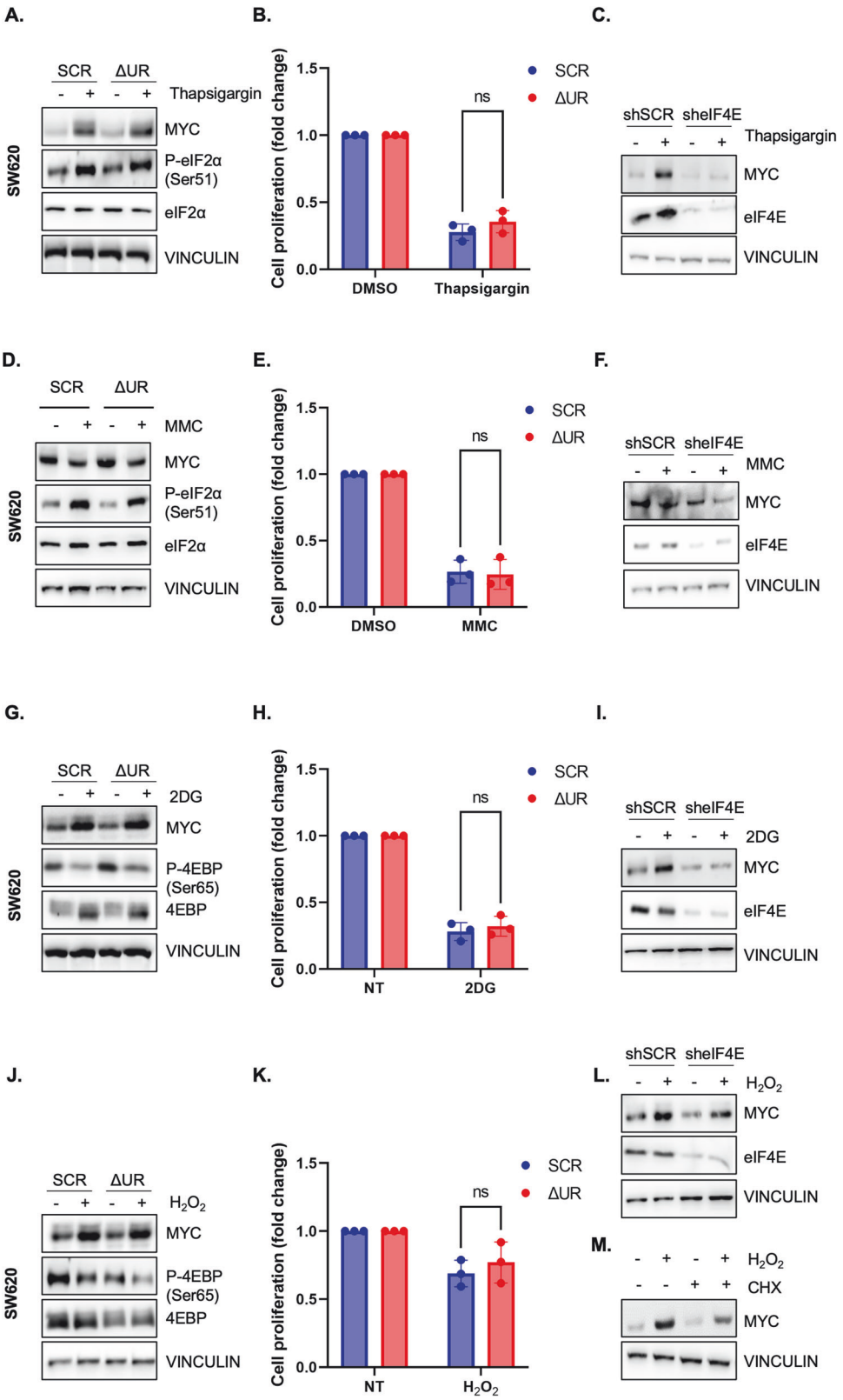

We first interfered the expression of the cap-binding protein eIF4E, a critical component of cap-dependent translation that was found to be dispensable for IRES-mediated translation of MYC [36, 37].

Ablation of eIF4E with two different shRNAs caused a robust decrease of endogenous MYC protein content, regardless of the presence of the IRES (Fig. 1D). Consistently, overexpression of a mutated 4EBP missing its 4 phosphorylation residues (4XALA) [38], thus acting as a dominant negative on the endogenous eIF4E inhibitor 4EBP, gave similar results (Fig. 1F) compared to eIF4E ablation, supporting the conclusion that the IRES sequence does

Fig. 2 MYC UR does not regulate MYC content or cell proliferation in response to various cell stress. A Immunoblot showing SW620 SCR and ΔUR cells treated with 0.5 μM thapsigargin or vehicle (DMSO) for 3 h. **B** SW620 SCR and ΔUR cells were treated with 0.5 μM thapsigargin or vehicle (DMSO) and counted after 48 h. Cell proliferation is expressed as fold change relative to DMSO treated cells (n = 3). **C** Immunoblot analysis of MYC protein levels after lentiviral mediated knockdown of eIF4E (sheIF4E) or control (shSCR) in SW620 for 72 h and treatment with 0.5 μM thapsigargin or vehicle (DMSO) for 3 h. **D** Immunoblot of the indicated proteins in SW620 SCR and ΔUR cells treated with 2 μM mitomycin C (MMC) or vehicle (DMSO) for 24 h. **E** Proliferation assay in SW620 SCR and ΔUR cells treated with 2 μM MMC or vehicle (DMSO) for 24 h. Data are expressed as fold change relative to DMSO treated cells (n = 3). **F** Immunoblot of the indicated proteins after eIF4E lentiviral mediated knockdown (sheIF4E) or control (shSCR) for 72 h in SW620 cells then treated with 2 μM MMC or vehicle (DMSO) for 24 h. **G** Immunoblot of SW620 SCR and ΔUR cells treated with 25 mM 2-deoxy-D-glucose (2DG) or vehicle (H_2O) for 16 h. **H** Proliferation assay in SW620 ΔUR or control cells treated with 25 mM 2DG or vehicle (H_2O) for 48 h. Cell proliferation is represented as fold change relative to vehicle-treated (NT) cells (n = 3). **I** Immunoblot of the indicated proteins after lentiviral-mediated knockdown of eIF4E (sheIF4E) or control (shSCR) in SW620 cells for 72 h followed by treatment with 25 mM 2DG or vehicle (H_2O) for 16 h. **J** Immunoblot of SW620 SCR and ΔUR cells after treatment with 150 μM hydrogen peroxide (H_2O_2) or vehicle (H_2O) for 3 h. **K** Cell proliferation assay of SW620 cells treated with 10 μM H_2O_2 or vehicle (H_2O) for 24 h. Cell proliferation is represented as fold change relative to vehicle-treated (NT) cells (n = 3). **L** Immunoblot of SW620 cells after 72 h of lentiviral-mediated knockdown of eIF4E (sheIF4E) and then treated with 150 μM H_2O_2 or vehicle (H_2O) for 3 h. **M** Immunoblot of SW620 SCR and ΔUR cells pre-treated for 5 min with 100 μg/mL cycloheximide (CHX) or vehicle (DMSO), then 30 min with 150 μM H_2O_2 or vehicle (H_2O). Data represent the mean ± SD of at least three experiments, each performed in triplicate. ns=not significant ($p > 0.05$) by Two-way ANOVA followed by post-hoc Tukey's multivariate analysis.

not affect MYC content in the absence of the cap-binding factor eIF4E. Furthermore, no difference in cell proliferation was observed across experiments with knockdown of eIF4E (Fig. 1E) nor overexpression of 4EBP 4XALA (Fig. 1G), demonstrating that MYC expression reflects cell proliferation and that the presence of MYC IRES does not balance the decrease of CRC cell proliferation resulting from attenuation of cap-dependent translation.

Following this, we investigated two other factors of the eIF4F initiation complex, eIF4A and eIF4G. eIF4A in particular was suggested to be critical for cap-independent translation of MYC [36]; lentiviral-mediated transduction of our two different small-hairpin RNAs provided more than 90% reduction of eIF4A1 mRNA (Supplementary Fig. 1C) and was accompanied by a reduction in MYC protein, a response that was identical in ΔUR and SCR cell lines (Fig. 1H), thus ruling out that an additional fraction of MYC translation could be generated from eIF4A acting at the IRES region. Similar results were observed for eIF4G using the same small-hairpin method and with similar efficacy of knockdown (Fig. 1I and Supplementary Fig. 1D).

Consistent with the inability of the MYC IRES region to mediate translational initiation independently of the cap, transfection of in vitro transcribed monocistronic luciferase mRNA with a defective cap analog (AP3G) and a hairpin in the 5′UTR preventing ribosomal scanning from the cap, failed to be translated in HCT116 cells, despite the presence of MYC IRES within the luciferase 5′UTR (Fig. 1J).

Taken together, these observations demonstrate that the region considered as MYC IRES cannot mediate cap-independent translation of MYC in cells grown under standard culturing conditions as previously argued [39], and fails to sustain cell viability when the general cap-dependent protein synthesis is inhibited.

The region corresponding to MYC IRES does not regulate MYC levels or resistance to cellular stress

We next sought to understand if the presumed IRES region is involved in the response to different cellular stress to support survival under unfavorable conditions.

Previous studies [33] demonstrated that exposing multiple myeloma cells to endoplasmic reticulum stress inducers, such as thapsigargin or tunicamycin, caused an increase of MYC expression via IRES translation, although general protein synthesis was inhibited [40]. We observed that in response to thapsigargin, MYC protein levels were upregulated in SW620 (Fig. 2A) or unchanged in HCT116 cells (Supplementary Fig. 2A) in both SCR and IRES-deleted clones. Since eIF2α phosphorylation was increased after thapsigargin treatment, these results indicate that MYC biosynthesis is increased or maintained when general protein translation is inhibited and that this effect is independent of the IRES. Since thapsigargin inhibited cell proliferation to the same extent in SCR and IRES-deleted cells (Fig. 2B and Supplementary Fig. 2B), these data demonstrate that the IRES region is not involved in the regulation of MYC levels and cell proliferation in response to ER stress. Further supporting a cap-dependent mechanism for ER stress-induced MYC regulation, knockdown of eIF4E disrupted MYC content in response to thapsigargin (Fig. 2C).

We next investigated the effects of the genotoxic stressors on MYC translation and cell proliferation. Subkhankulova and colleagues [23] showed that MYC IRES-mediated translation was activated in response to DNA damage and genotoxic stress induced by the DNA alkylating drug mitomycin C (MMC) to maintain intracellular MYC content and cancer cell viability. In keeping with these findings, after treatment of SW620 and HCT116 cells with MMC, cell proliferation and MYC protein content were reduced, although not abrogated, while p-eIF2α was increased (Fig. 2D and Supplementary Fig. 2C). However, in ΔUR cells residual MYC protein levels were also detected, cell proliferation was inhibited at levels comparable to SCR cells (Fig. 2D, E and Supplementary Fig. 2C, D), and knockdown of eIF4E abrogated the residual MYC protein content (Fig. 2F), indicating that MYC translation and cell viability under genotoxic stress are not sustained by an IRES-dependent mechanism.

We then tried to address whether oxidative and metabolic stressors, characteristic of the tumor microenvironment, could exploit IRES-dependent translation to support MYC expression and CRC growth. As expected, both 2-deoxy-D-glucose (2DG), a glucose analog that is not metabolizable, and hydrogen peroxide (H_2O_2) treatment inhibited the regulator of global protein translation mTOR, as documented by a decrease of 4EBP phosphorylation (Fig. 2G, J and Supplementary Fig. 2E, G). In SW620 cells both treatments resulted in up-regulation of MYC protein levels (Fig. 2G, J) and in a decrease of CRC cell proliferation (Fig. 2H, K). However, these effects were not mediated by IRES translation, as the same upregulation of MYC was observed also in the cells lacking the IRES sequence (Fig. 2G, J) and the sensitivity of ΔUR cells to 2DG and H_2O_2 was not significantly accentuated compared to control cells (Fig. 2H, K).

Interestingly, while 2DG-induced MYC upregulation was prevented by ablation of eIF4E (Fig. 2I), the increased levels of MYC following oxidative stress were not altered by neither eIF4E knockdown nor inhibition of general protein synthesis with cycloheximide (CHX) (Fig. 2L, M), suggesting that the latter form of stress promotes MYC stabilization rather than its translation.

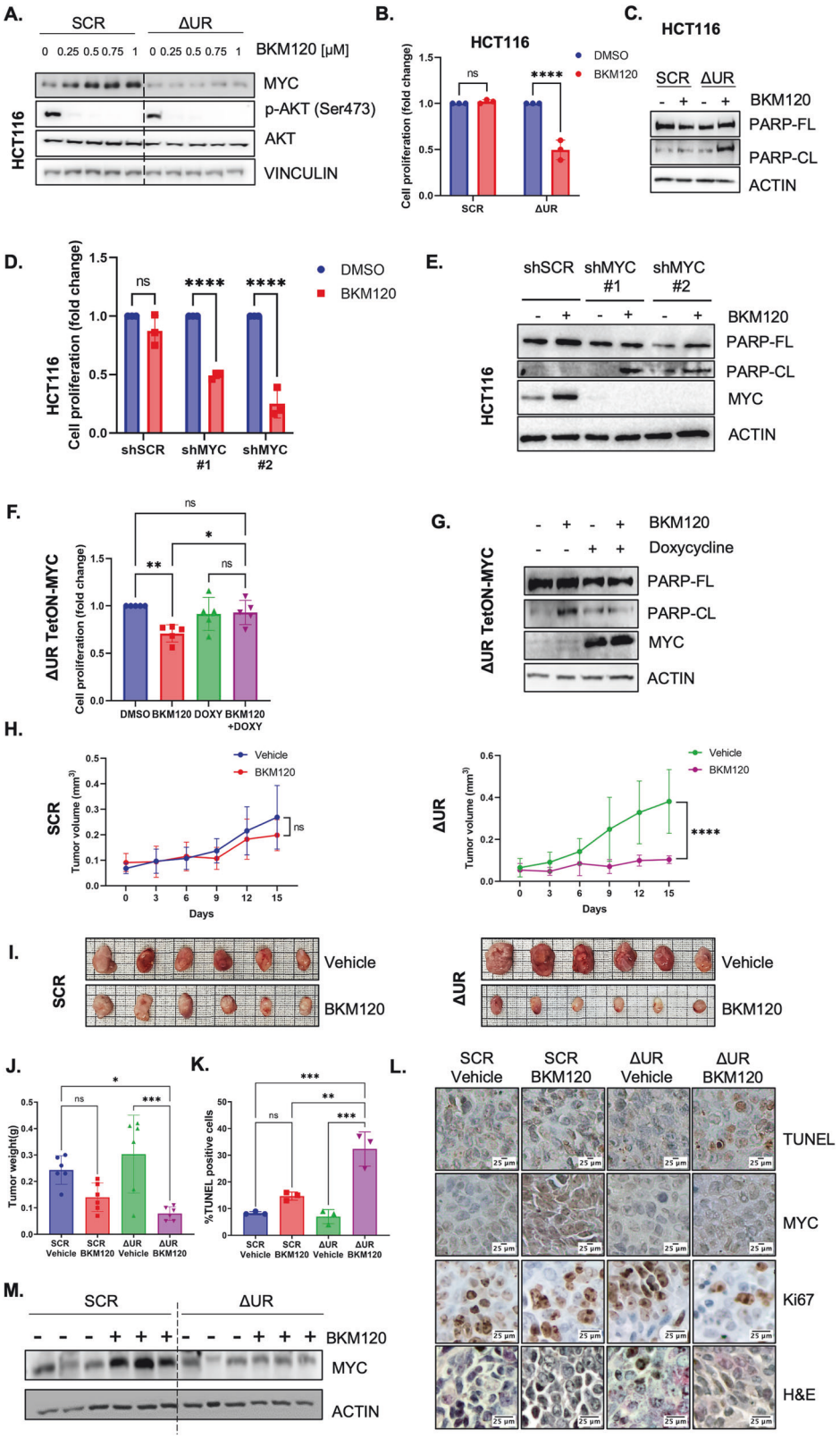

MYC upregulation and decreased cell proliferation also occurred in SCR and IRES-deleted HCT116 cells treated with 2DG (Supplementary Fig. 2E, F), whereas H_2O_2 did not induce upregulation of MYC and caused reduction of cell proliferation also in this context along with inhibition of general protein synthesis (Supplementary Fig. 2G, H).

Overall, our results demonstrate that the presence of the sequence considered as MYC IRES does not regulate MYC

Fig. 3 MYC UR provides resistance to PI3K inhibition. A Immunoblot of HCT116 SCR and ΔUR cells treated with DMSO (0) or BKM120 at the indicated concentrations for 24 h and stained with the indicated antibodies. **B** HCT116 SCR and ΔUR cells were treated with 0.5 μM BKM120 and counted after 48 h. Data are shown as fold change relative to vehicle (DMSO) treated cells (n = 3). **C** Immunoblot of Poly ADP-Ribose Polymerase-1 (PARP) full length (FL) or cleaved (CL) in HCT116 SCR and ΔUR cells treated with 1 μM BKM120 or vehicle (DMSO) for 48 h. β-actin, loading control. **D** Cell proliferation assay in HCT116 cells expressing two different MYC shRNAs, treated with 0.5 μM BKM120 or vehicle (DMSO) for 72 h. Cell proliferation is represented as fold change relative to DMSO-treated cells (n = 3). **E** Immunoblot of HCT116 cells expressing two different MYC shRNAs and control (shSCR), and treated with 1 μM BKM120 or vehicle (DMSO) for 24 h. **F** Cell proliferation assay using HCT116 ΔUR cells infected with a doxycycline-inducible lentivirus overexpressing human MYC coding sequence (ΔUR TetON-MYC). After selection with puromycin, cells were treated with 0.5 μM BKM120 and/or 1 μg/mL doxycycline (DOXY) or vehicle (BKM120: DMSO; doxycycline: H_2O) for 72 h. Cell proliferation is represented as fold change relative to DMSO-treated cells (n = 5). **G** Immunoblot of HCT116 ΔUR TetON-MYC cells treated with 1 μM BKM120 and/or 1 μg/mL doxycycline (DOXY) or vehicle (BKM120: DMSO; doxycycline: H_2O) for 24 h. **H** Tumor growth over time of HCT116 SCR (left panel) and ΔUR (right panel) cells subcutaneously implanted in the flanks of CD1 nude mice measured every three days (n = 6). **I** Photographs of HCT116 SCR (left panel) and ΔUR (right panel) cell tumor masses explanted at the end of the xenograft experiment. **J** Weight of the tumor masses of HCT116 SCR and ΔUR cells explanted from mice flanks at the moment of sacrifice (n = 6). **K** Quantification of TUNEL-positive cells. The apoptotic ratio was defined as the fraction of TUNEL-positive cells per total cells counted. **L** Immunohistochemistry performed on the xenograft tumor masses previously fixed in formalin and paraffin embedded. Scale bar 25 μm. **M** Immunoblot performed using tumors from panel **I**. Data represent the mean ± SD of at least three experiments, each performed in triplicate. ns=not significant ($p > 0.05$), *$p < 0.05$, **$p < 0.01$, ****$p < 0.000,1$ by One-way ANOVA followed by post-hoc Tukey's multivariate analysis.

translation and tumor cell proliferation in response to stress. Therefore, from here on, we will refer to this sequence as MYC upstream region (MYC UR).

MYC UR induces MYC upregulation and confers resistance to PI3K inhibition

A previous study [37] showed that the dual PI3K/mTOR inhibitor BEZ-235 increases MYC protein content, an effect that was attributed to the engagement of MYC IRES-translation [37, 41]. Based on these results, we studied the effect of increasing doses of the clinically tested pan-class I PI3K inhibitor BKM120 [42], in PI3K-mutated SCR and ΔUR HCT116 cells. MYC protein content was significantly upregulated by PI3K inhibition in SCR, but not in ΔUR cells (Fig. 3A). The efficacy of inhibition of the PI3K pathway was confirmed by the abrogation of AKT phosphorylation. Similarly, shRNA-mediated deletion of PI3K caused a robust increase of MYC protein content in SCR but not in ΔUR cells (Supplementary Fig. 3A). The activity of PI3K signaling in SCR and ΔUR cells did not appear to be different (Fig. 3A).

We next wondered whether this mechanism is involved in conferring resistance to PI3K inhibitors. As shown in Fig. 3B, the proliferation rate of SCR cells was not significantly affected by BKM120, whereas it was robustly reduced in ΔUR cells. Accompanying the reduced proliferation, we observed increased apoptosis in ΔUR cells, documented by the increase of PARP cleavage compared to SCR cells (Fig. 3C).

Upon shRNA-mediated knockdown of MYC, control cells became sensitive to BKM120-mediated inhibition (Fig. 3D), and this was associated to increased PARP cleavage (Fig. 3E). By contrast, overexpression of MYC in UR-deleted cells restored resistance to PI3K inhibitors (Fig. 3F) and prevented apoptosis (Fig. 3G), demonstrating that MYC is required for the differential response of SCR and UR-deleted cells to PI3K inhibition.

Next, we grafted SCR and ΔUR cells into the flanks of athymic nude mice, and when tumors reached the volume of 100 mm^3, we treated mice with 30 mg/kg BKM120 via oral gavage for an additional 15 days.

As shown in Fig. 3H, SCR tumors treated with BKM120 did not show a significant difference of the growth rate when compared to tumors treated with vehicle control. At the end of the experiment, their volumes and weights were not significantly different (Fig. 3I, J), the percentage of TUNEL-positive cells demonstrated no significant elevation (Fig. 3K, L), there was a similar expression of Ki67 (Fig. 3L), and MYC content was significantly induced (Fig. 3L, M). By contrast, treatment with BKM120 robustly inhibited the growth of ΔUR tumors (Fig. 3H, I), significantly increased the percentage of TUNEL-positive cells (Fig. 3K, L) alongside a decrease of Ki67 positive cells (Fig. 3L), while it did not change the levels of MYC (Fig. 3L, M).

Collectively, these data demonstrate that MYC UR confers resistance to PI3K inhibitors in CRC models by upregulating MYC content, an effect that can be abrogated by deletion of the UR.

PI3K inhibition promotes the increase of MYC content via FOXO3a-dependent transcription and stabilization

We next investigated the UR-mediated mechanism of MYC upregulation in response to PI3K inhibitors.

Interference of eIF4E completely inhibited the induction of MYC protein in the presence of BKM120 (Fig. 4A), supporting previous observations [43], and demonstrating that the BKM120-induced upregulation of MYC is mediated by MYC UR (Fig. 3A), but not through a cap-independent mechanism.

To determine if BKM120 induces changes in MYC mRNA translation, we performed polysomal fractionation. While the association of MYC mRNA to polyribosomes was not significantly changed in both BKM120-treated SCR and ΔUR cells (Fig. 4B), there was a decrease of global translation efficiency (as defined by the ratio of polysome:monosome association) in both SCR and ΔUR cells treated with BKM120 (Supplementary Fig. 4A). In addition, the association of β-actin mRNA specifically with polysomes was decreased (Supplementary Fig. 4B) and the phosphorylation levels of 4EBP and S6 were reduced in response to the drug (Supplementary Fig. 4C). Therefore, these data suggest that while general initiation is inhibited, MYC translation is maintained, and its mRNA content increased. Consistent with this possibility, treatment with BKM120 significantly induced MYC mRNA levels in SCR but not in ΔUR cells (Fig. 4C).

Analysis of cells treated with the transcriptional inhibitor actinomycin D (ActD) showed no difference in MYC mRNA stability between control and BKM120-treated SCR and ΔUR cells (Supplementary Fig. 4D), thus indicating that BKM120 could induce MYC transcription.

To further validate this observation, we transfected CRC cells with a luciferase reporter vector containing MYC promoter with or without the UR region (Fig. 4D) and tested the response to PI3K inhibition by luciferase assay. Treatment with BKM120 induced a significant increase of luminescence only in cells transfected with the reporter plasmid containing MYC UR, but not in those transfected with the construct lacking this region (Fig. 4D). Also, ActD prevented the BKM120-mediated increase of luciferase activity (Supplementary Fig. 4E), confirming that PI3K inhibition increases MYC transcription through the UR region.

Previous observations indicated that FOXO3a, a member of the Forkhead box O (FOXO) family of transcription factors and predominantly expressed in colorectal tumor cells is required for

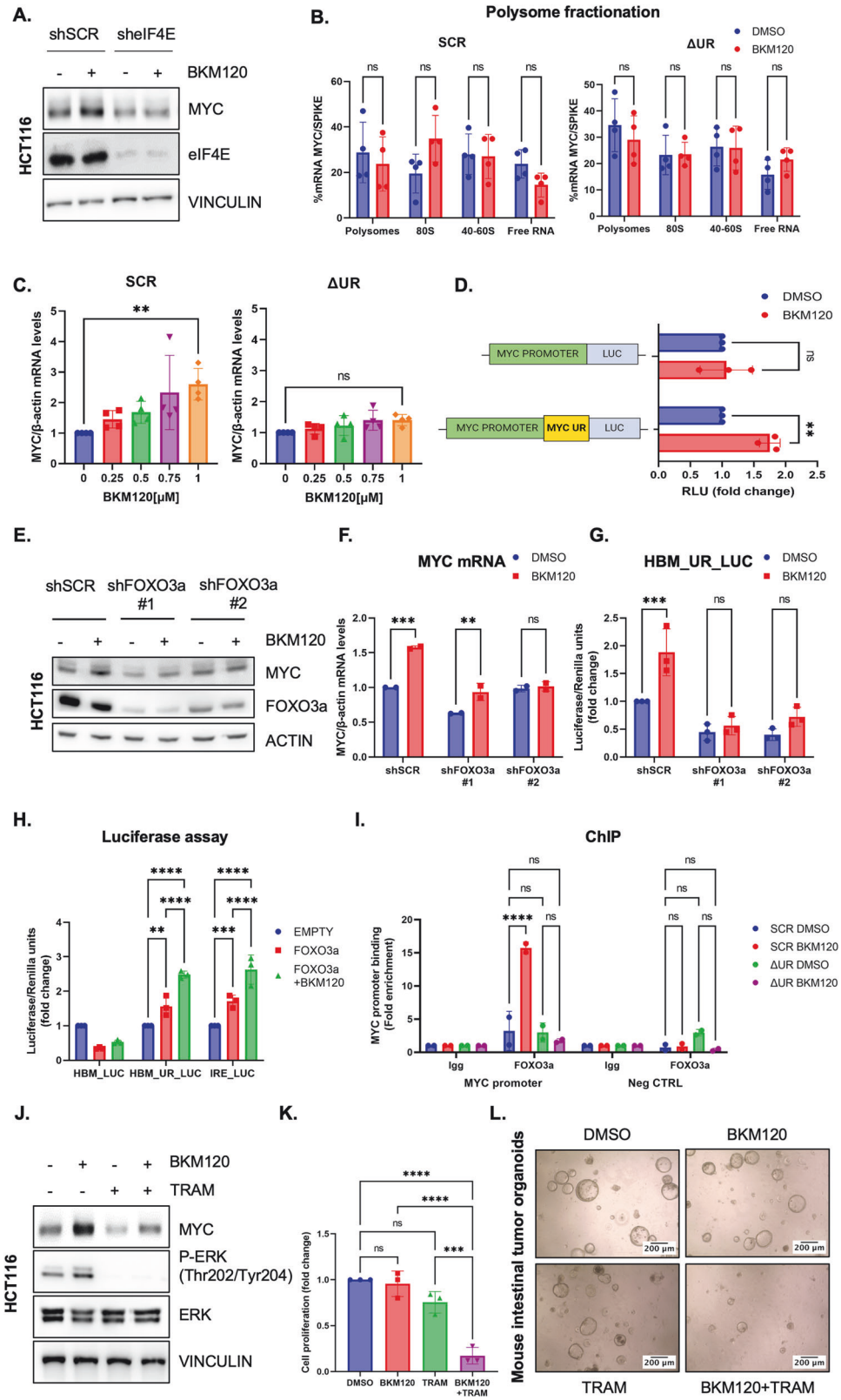

the elevation of MYC content in response to the dual PI3K/mTOR inhibitor BEZ-235 [37]. Based on these observations, we tested if FOXO3a could be involved in the observed transcriptional response of MYC to BKM120 through the UR. Consistent with this hypothesis, knockdown of FOXO3a abrogated BKM120-induced upregulation of MYC protein and mRNA, as well as the BKM120-mediated increase of luciferase activity of the reported construct containing MYC promoter and the UR region (HBM_UR_LUC) (Fig. 4E–G).

Fig. 4 PI3K inhibition enhances MYC transcription via MYC UR. A Immunoblot of HCT116 cells after lentiviral mediated knockdown of eIF4E (sheIF4E) or control (shSCR) for 72 h, then treated with 1 μM BKM120 or vehicle (DMSO) for 24 h. **B** QPCR analysis of MYC mRNA after polysome fractionation of HCT116 SCR and ΔUR cells treated with 1 μM BKM120 or vehicle (DMSO) for 24 h. A synthetic spike-in RNA was added to each fraction before RNA extraction and used as loading control (n = 4). **C** QPCR analysis of MYC mRNA in HCT116 SCR and ΔUR cells treated with BKM120 or vehicle (DMSO, point 0) at the indicated concentrations for 24 h. β-actin mRNA levels were used to normalize the data (n = 4). **D** Luciferase assay performed in HCT116 cells transfected with a plasmid harboring the luciferase reporter gene under the control of MYC promoter (HBM_LUC) or the same plasmid with MYC UR region inserted between MYC promoter and the luciferase open reading frame (HBM_UR_LUC) (left panel) and treated with 1 μM BKM120 or vehicle (DMSO) for 24 h (right panel) (n = 3). Left panel created in BioRender. **E** Immunoblot showing HCT116 cells after lentiviral mediated knockdown of FOXO3a with two different shRNAs (shFOXO3a#1 and shFOXO3a#2) or control (shSCR) and treated with 1 μM BKM120 or vehicle (DMSO) for 24 h (n = 2). **F** QPCR analysis performed in HCT116 cells described in panel E to evaluate MYC mRNA expression levels. β-actin mRNA levels were used to normalize the data (n = 2). **G** Luciferase assay performed in HCT116 cells after lentiviral mediated knockdown of control (shSCR) or two different shRNAs targeting FOXO3a (shFOXO3a#1 and shFOXO3a#2), then transfected with HBM_UR_LUC plasmid and treated with 1 μM BKM120 or vehicle (DMSO) for 24 h (n = 3). **H** Luciferase assay in HCT116 cells transfected with HBM_LUC, HBM_UR_LUC, or IRE_LUC as a positive control and co-transfected with a vector expressing human FOXO3a and/or treated with 1 μM BKM120 or vehicle (DMSO) for 24 h (n = 3). **I** Chromatin immunoprecipitation performed in HCT116 SCR and ΔUR cells. FOXO3a recruitment after 24 h administration of 1 μM BKM120 or vehicle (DMSO) is shown on MYC promoter or on a 5000 bp region located upstream the FOXO3a binding site on MYC promoter used as negative control (n = 2). **J** Immunoblot of HCT116 SCR and ΔUR cells treated for 24 h with vehicle (DMSO), 1 μM BKM120, 10 nM trametinib (TRAM) or a combination of the two drugs. **K** Proliferation assay of HCT116 cells treated for 48 h with vehicle (DMSO), 0.5 μM BKM120, 5 nM trametinib (TRAM) or a combination of BKM120 and TRAM at the same concentrations (n = 3). **L** Representative images of intestinal tumor organoids isolated from the small intestine of $APC^{Min/+}$ mice and treated with vehicle (DMSO), 0.5 μM BKM120, 5 nM trametinib (TRAM) or BKM120 and TRAM in combination for 72 h. Data represent the mean ± SD of at least three experiments, each performed in triplicate. ns=not significant ($p > 0.05$), *$p < 0.05$, **$p < 0.01$, ****$p < 0.000,1$ by One-way ANOVA followed by post-hoc Tukey's multivariate analysis.

Overexpression of FOXO3a increased the activity of the same construct, and of a luciferase reporter construct containing a canonical FOXO binding site (insulin response element, IRE) in its promoter region, and the increase was further enhanced by BKM120 treatment. Conversely, exogenous FOXO3a failed to increase the activity of a promoter construct containing MYC promoter but lacking the UR region (Fig. 4H).

Chromatin immunoprecipitation (ChIP) experiments demonstrated that FOXO3a is recruited over to the MYC promoter, and that the association is increased by BKM120 in SCR but not in UR-deficient cells (Fig. 4I).

Collectively, these data demonstrate that the increase of MYC mRNA in response to BKM120 is mediated by FOXO3a and requires the UR region.

Since it was shown that dual PI3K/mTOR blockade also causes a FOXO3a-mediated increase of MYC protein content through a crosstalk with MEK-MAPK axis [37], we wondered whether this mechanism contributes to the elevation of MYC protein levels in response to PI3K inhibition.

In keeping with this hypothesis, treatment with BKM120 caused increased phosphorylation of the MEK1 substrate ERK and MYC upregulation, while MEK inhibition with the clinically approved MEK1/2 inhibitor trametinib [44] prevented the increase of MYC protein (Fig. 4J). Since the BKM-induced elevation of MYC mRNA was not modified by MEK inhibition (Supplementary Fig. 4F), we hypothesized that MAPK signaling could increase MYC levels by enhancing protein stability. Consistent with this idea, the half-life of MYC in BKM120-treated cells was significantly reduced by trametinib (Supplementary Fig. 4G).

Supporting the notion that this MEK-mediated crosstalk contributes to the resistance to PI3K inhibition, treatment of human CRC cells or mouse intestinal tumor organoids with BKM120 failed to inhibit cell proliferation, while co-incubation with trametinib induced a strong antiproliferative response in both models (Fig. 4K, L and Supplementary Fig. 4H).

Together, these findings demonstrate that BKM120 promotes an increase of MYC content via FOXO3a-dependent transcription and stabilization, a process that confers resistance to PI3K inhibitors and requires the UR region.

MYC UR promotes resistance to PI3K inhibitors by inducing an autophagic response

We next sought to understand how the UR-induced upregulation of MYC confers resistance to BKM120. Since previous works suggest that a common mechanism to escape the antitumor effect of targeted drugs, including PI3K inhibitors, is the induction of autophagy [45–48], we wondered whether MYC UR is connected to this cellular process.

Staining with lysotracker probes showed that BKM120 strongly enhanced acidic cellular organelles in SCR, but not in ΔUR cells, suggesting that the drug induces autophagy-associated lysosomal activity only in the presence of the UR (Fig. 5A).

To confirm that the observed effect could be attributed to increased autophagic flux and formation of autolysosomes, we used the mCherry-GFP-LC3 reporter system [49]. Treatment with BKM120 significantly increased the number of red puncta (autolysosomes) in SCR but not ΔUR cells, while the autophagy inhibitor bafilomycin A, used as control, enhanced the formation of yellow puncta (autophagosomes), demonstrating that PI3K blockade increases the autophagic flux via MYC UR (Fig. 5B). Consistently, the protein p62, which is degraded when autophagy is induced [50], was reduced after BKM120 treatment in SCR cells, while it was unchanged in cells lacking the MYC UR (Fig. 5C). As expected, this reduction in p62 protein levels in response to BKM120 treatment was not due to decreased transcription (Supplementary Fig. 5A).

To ascertain that BKM120-induced autophagy requires the upregulation of MYC, we ablated MYC expression through its lentiviral-mediated knockdown. BKM120 failed to induce autophagy and p62 downregulation in MYC-deficient cells (Fig. 5D, E).

Accordingly, overexpression of MYC restored the autophagic response (Fig. 5F) and decreased p62 protein levels (Fig. 5G) in BKM120-treated UR-deleted cells.

Together, these data demonstrate that the UR-mediated upregulation of MYC that follows PI3K inhibition (Fig. 5C) induces an autophagic response that sustains drug resistance.

Since previous studies found that MYC occupies a cluster of autophagy-related gene promoters [51], we measured the levels of these target genes in BKM120-treated vs untreated cells. As shown in Fig. 5H, all these transcripts were induced by BKM120 treatment in SCR, but not in ΔUR cells, indicating their possible involvement in the observed effect.

Inhibition of UR-mediated autophagy overcomes resistance to PI3K inhibitors

Having found that MYC-induced autophagy is the key mechanism responsible for resistance to BKM120, we asked if blockade of this mechanism could provide therapeutic benefit in CRC models.

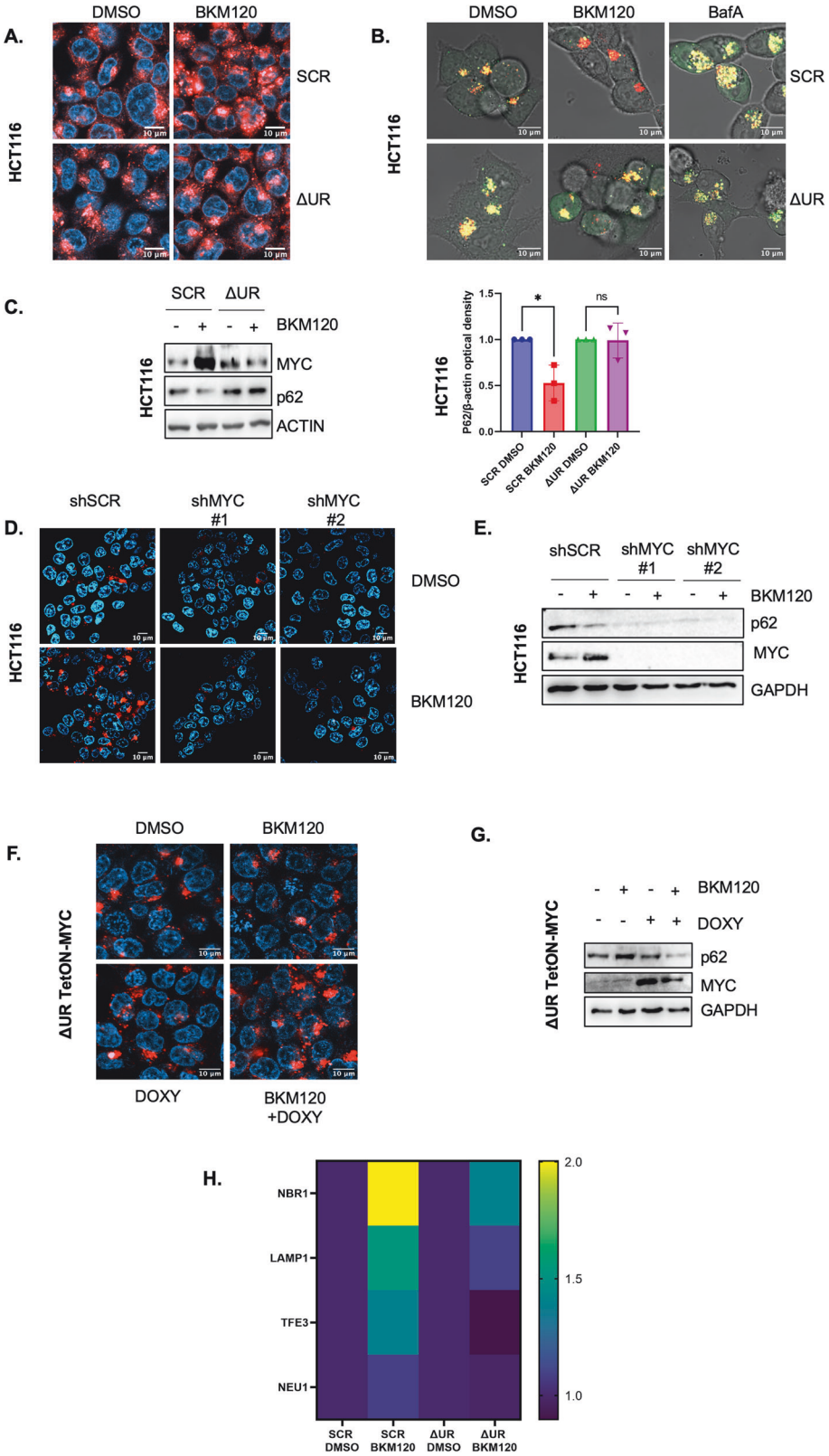

Exposure of PI3K-resistant human HCT116 CRC cells (Fig. 6A, C) or mouse tumor intestinal organoids (Fig. 6E) to the autophagy inhibitors bafilomycin A (BafA) or chloroquine (CQ) abrogated the resistance to PI3K inhibition and induced apoptotic cell death (Fig. 6B, D).

To validate these observations in relevant pathophysiological models, we tested CRC stem cells derived from five different patients [52]. We found that two of them were resistant to PI3K inhibition and that the response correlated with the levels of MYC, being higher and upregulated by BKM120 in the two

Fig. 5 Resistance of CRC cells to PI3K inhibitors is linked to MYC-mediated increase of autophagy. A Representative confocal images of HCT116 SCR and ΔUR cells treated with 1 μM BKM120 or vehicle (DMSO) for 24 h and stained with the fluorescently labeled lysosomal probe Lysotracker Red 30 min before imaging. DAPI (blue) was used to counterstain nuclei (Scale bar 10 μm). **B** Representative confocal images of HCT116 SCR and ΔUR cells transduced with the lentivirus expressing the mCherry-GFP-LC3 and treated with vehicle (DMSO), 1 μM BKM120, or 10 nM bafilomycin A (BafA) for 24 h. Yellow puncta indicate autophagosomes (mCherry + /GFP +) while autolysosomes are in red (mCherry + /GFP −). Scale bar 10 μm. **C** Left panel: Immunoblot showing HCT116 SCR and ΔUR cells treated with 1 μM BKM120 for 24 h or vehicle (DMSO); Right panel: Densitometric analysis representing p62/β-actin optical density of three independent experiments. **D** Representative confocal images of HCT116 cells after MYC lentiviral mediated knockdown with two different shRNAs (shMYC#1 and #2) or control (shSCR) for 72 h then treated with 1 μM BKM120, or vehicle (DMSO) for 24 h and stained with the fluorescently labeled lysosomal probe Lysotracker Red 30 min before imaging. DAPI (blue) is a nuclear counterstain. Scale bar 10 μm. **E** Immunoblot showing HCT116 cells treated with vehicle (DMSO) or 1 μM BKM120 for 24 h after two different lentiviral-mediated knockdowns of MYC for 72 h. **F** Representative confocal images of HCT116 ΔUR cells transduced with a lentivirus expressing doxycycline-inducible MYC coding sequence and selected with puromycin to obtain a stable cell line (ΔUR TetON-MYC). Cells were treated with either vehicle (BKM120: DMSO; doxycycline: H_2O), 1 μM BKM120 and/or 1 μg/mL doxycycline to induce MYC expression. Lysotracker Red was added 30 min before imaging and DAPI (blue) is a nuclear counterstain. Scale bar 10 μm. **G** Immunoblot of HCT116 ΔUR TetON-MYC cells treated with 1 μM BKM120 and/or 1 μg/mL doxycycline or vehicle (BKM120: DMSO; doxycycline: H_2O) for 24 h. **H** Heatmap of mRNA expression analyzed by QPCR of autophagy-related genes (NBR1, LAMP-1, TFE3, and NEU1) relative to β-actin in HCT116 SCR and ΔUR cells treated with vehicle (DMSO) or 1 μM BKM120 for 24 h (n = 3). Data represent the mean ± SD of at least three experiments, each performed in triplicate. ns=not significant ($p > 0.05$), *$p < 0.05$, **$p < 0.01$, ****$p < 0.000,1$ by One-way ANOVA followed by post-hoc Tukey's multivariate analysis.

resistant clones (Supplementary Fig. 6A, B, C). We selected clone 21 (CSphC#21) and tested their response to PI3K and autophagy inhibitors. In agreement with our findings, treatment of CSphC#21 with BKM120 induced a decrease of p62 protein content (Fig. 6F) and neither BKM120 nor chloroquine administered individually significantly altered cell proliferation or tumorsphere formation, while the combination resulted in a robust inhibition of proliferation and sphere-forming capability (Fig. 6G and Supplementary Fig. 6D). Likewise, the clone 21 cells grown in a three-dimensional scaffold of Matrigel demonstrated a similar sensitivity to the combination treatment of BKM120 and CQ, but to neither of the drugs individually (Fig. 6H, I).

We then grafted the cells into CD1 nude mice, and when tumors became palpable, animals were divided into 4 groups treated with: (1) 30 mg/kg BKM120, (2) 30 mg/kg chloroquine, (3) a combination of the two drugs, or (4) vehicle alone.

As shown in Fig. 6J, compared to vehicle and individual treatments, only the combination of BKM120 with CQ caused a significant reduction of tumor growth. The combination treatment was associated to a significant reduction of Ki67-positive cells and increased apoptosis, documented by the higher percentage of TUNEL-positive cells (Fig. 6K), as well as by the increase of PARP cleavage (Fig. 6L).

Collectively, these data demonstrate that inhibition of autophagy abrogates the resistance to PI3K inhibitors in preclinical models of CRC.

Resistance to PI3K inhibitors depends on MYC UR translocation in Burkitt Lymphoma cells

Once we defined the mechanism of resistance to PI3K inhibition, we hypothesized that Burkitt Lymphoma (BL) cells could be a pathophysiologically relevant model of MYC UR deletion because they frequently undergo a MYC/IGH t(8;14)(q24;q32) translocation [53] with or without the first exon of MYC, which contains the UR region.

Hence, we wondered if the response to various cellular stress inducers and the mechanisms of UR-mediated resistance to PI3K inhibitors could be validated in two cell lines characterized by the presence or absence of the translocated MYC UR: Raji and DG75 cells, respectively [54, 55] (Fig. 7A).

Treatment with the cell stressors thapsigargin, MMC, 2DG, and H_2O_2 caused a reduction of general translation and MYC protein levels (Supplementary Fig. 7A–H), likely because the mechanisms of the integrated stress response (IRS) that maintain MYC translation during stress are impaired after chromosomal rearrangements.

However, in keeping with the observations in CRC cells, MYC levels and the proliferation rate after various treatments were identical in UR-translocated and non-translocated cells, arguing against the possibility that this region could function as a key regulator of MYC translation and cell survival under stress also in this context.

Consistent with the data in CRC cells, in UR-translocated Raji cells, MYC protein and mRNA levels (Fig. 7B, C) as well as MYC-regulated autophagy targets (Fig. 7D) were induced by BKM120 treatment. Consequently, the autophagic flux was enhanced, as revealed by the increased lysotracker staining (Fig. 7E), of the red puncta after transduction of the lentivirus expressing mCherry-GFP-LC3 reporter (Fig. 7F), and the decreased p62 protein levels (Fig. 7G and Supplementary Fig. 7I). This MYC-induced increase of autophagic flux was associated to resistance to BKM120 that was counteracted when autophagy was inhibited with chloroquine (Fig. 7H) or bafilomycin A (Supplementary Fig. 7J) due to increased apoptosis (Fig. 7J). Conversely, in DG75 cells lacking MYC UR translocation, BKM120 alone induced a significant antiproliferative response (Fig. 7H) associated to apoptosis (Fig. 7I) and failed to upregulate MYC and its targets as well as to induce the autophagic response (Fig. 7B–7F). Notably, upon exogenous expression of MYC with a tetracycline-inducible vector, DG75 cells became resistant to BKM120 treatment (Fig. 7K) and autophagic flux was restored, as documented by the enhanced lysotracker staining (Fig. 7L) and decrease of p62 protein levels (Fig. 7M). Consequently, apoptosis was prevented, as shown by the unchanged levels of PARP cleavage (Fig. 7N).

Taken together, these results demonstrate that translocation of MYC UR along with its open reading frame (ORF) confers resistance to BKM120 treatment in BL cells, while in the absence of UR translocation, cells are vulnerable to PI3K inhibitors.

DISCUSSION

In the present work we have demonstrated that the portion of MYC referred as IRES, instead of regulating translational internal initiation, functions as a central transcriptional hub, mediating resistance of colorectal cancer cells to PI3K inhibitors.

Aberrant activation of PI3K/AKT signaling is a key tumorigenic event associated to 60–70% of CRC and may result from activating mutations of PI3K, increased extracellular TKR ligands, activated Ras, or loss of function of the phosphatase PTEN [56]. For this reason, many compounds inhibiting PI3K have been or are being developed and tested in preclinical models and in clinical trials of CRC [57].

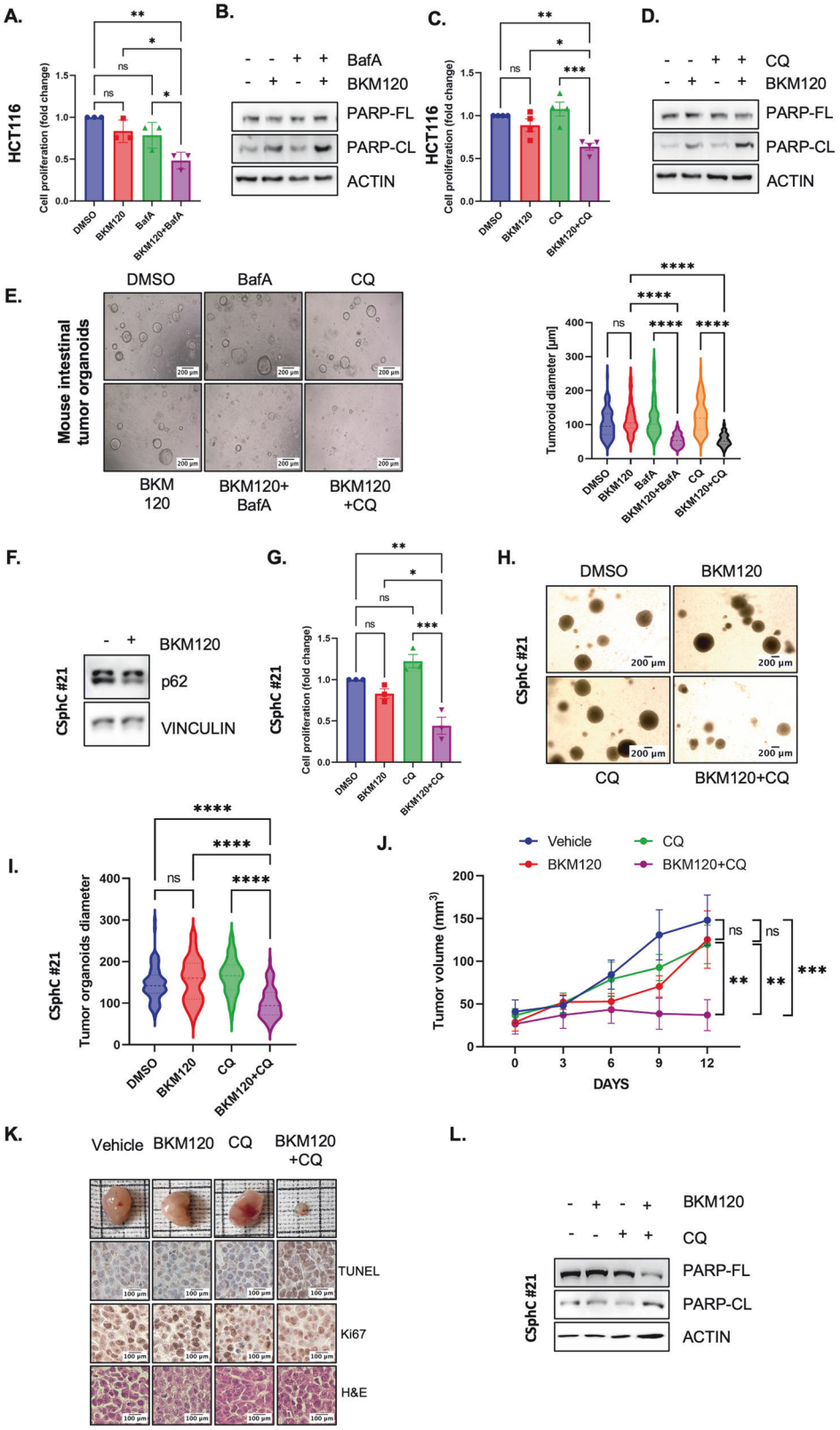

In most cases, PI3K inhibitors, including the pan-acting class I PI3K inhibitor BKM120 used in this study, have been tested in phase I clinical trials in CRC patients, alone or in combination, showing a good safety profile [56, 57]. However, due to the documented activation of compensatory mechanisms, leading to resistance, there is still concern about the efficacy of these drugs. In this work we have confirmed that BKM120 is inefficacious in preventing the growth of colorectal cancer cells and we have discovered that a key mechanism responsible of the observed drug resistance is the increase of autophagic flux.

Fig. 6 Autophagy blockade overcomes CRC resistance to PI3K inhibitors. A Proliferation assay of HCT116 cells treated with vehicle (DMSO), 0.5 μM BKM120, 2 nM bafilomycin A (BafA) or with the two drugs in combination (BKM120+BafA) for 72 h. Data are normalized to DMSO-treated cell number (n = 3). **B** Immunoblot documenting Poly ADP-Ribose Polymerase-1 (PARP) full length (FL) or cleaved (CL) in HCT116 SCR cells treated with vehicle (DMSO), 1 μM BKM120 and/or 4 nM bafilomycin A (BafA) for 72 h. **C** Proliferation assay of HCT116 cells treated with vehicle (BKM120: DMSO; CQ: H_2O), 0.5 μM BKM120, 2 nM chloroquine (CQ) or with the two drugs in combination (BKM120 + CQ) for 72 h. Data are normalized to DMSO-treated cell number (n = 4). **D** Immunoblot documenting Poly ADP-Ribose Polymerase-1 (PARP) full length (FL) or cleaved (CL) in HCT116 SCR cells treated with vehicle (BKM120: DMSO; CQ: H_2O), 1 μM BKM120 and/or 2 nM chloroquine (CQ) for 72 h. **E** Left panel: Representative images of intestinal tumor organoids isolated from the small intestine of $APC^{Min+/-}$ mice treated with vehicle (BKM120, BafA: DMSO; CQ: H_2O), 0.5 μM BKM120, 2 nM bafilomycn A (BafA), 2 nM chloroquine (CQ) and BKM120 in combination with BafA or CQ for 48 h. Right panel: Distribution of intestinal tumor organoids diameters measured using ImageJ. **F** Immunoblot of human tumorspheres (CSphC#21) derived from a patient with colorectal cancer treated with 1 μM BKM120 or vehicle (DMSO) for 24 h. **G** Proliferation assay in human tumorspheres (CSphC#21) derived from a colorectal cancer patient treated for 72 h with vehicle (BKM120: DMSO; CQ: H_2O), 0.5 μM BKM120, 2 nM chloroquine, and the two drugs in combination. Data are expressed as fold change relative to DMSO-treated cells (n = 3). **H** Representative images of human tumor organoids derived by 3D-cultured CSphC#21 in a Matrigel scaffold then treated with vehicle (BKM120: DMSO; CQ: H_2O), 0.5 μM BKM120, 2 nM CQ, or in combination for 72 h. Scale bar 200 μm. **I** Distribution of diameters of tumor organoids derived by 3D-cultured CSphC#21 in a Matrigel scaffold then treated with vehicle (BKM120: DMSO; CQ: H_2O), 0.5 μM BKM120, 2 nM CQ, or in combination for 72 h. Scale bar 200 μm. Organoid diameters measured using ImageJ. **J** Tumor growth over time of CSphC#21 subcutaneously implanted in the flanks of CD1 nude mice measured every three days. Mice were daily treated with 30 mg/kg BKM120 dissolved in 90% corn oil, 10% DMSO by oral gavage and/or 30 mg/kg chloroquine (CQ) in saline by IP injection, or vehicle (BKM120: 90% corn oil, 10% DMSO oral gavage; CQ: 0.9% normal saline IP injection). **K** Representative pictures of CSphC#21 tumors at the day of sacrifice, TUNEL assay documenting cell death and immunohistochemistry for Ki67 performed on tumor masses previously fixed in formalin and paraffin embedded. H&E: Hematoxylin and Eosin. Scale bar 100 μm. **L** Immunoblot documenting full length (FL) and cleaved (CL) PARP levels of the tumors from the patient-derived xenograft described in panel **J**. Data represent the mean ± SD of at least three experiments, each performed in triplicate. ns = not significant ($p > 0.05$), *$p < 0.05$, **$p < 0.01$, ***$p < 0.001$ ****$p < 0.000,1$ by One-way ANOVA followed by post hoc Tukey's multivariate analysis.

Many observations have shown that autophagy is an important mechanism exploited by cancer cells to survive to chemotherapy and targeted therapy [58], leading to the conclusion that targeting autophagy with specific inhibitors might represent a valuable strategy to overcome drug resistance [59].

Consistent with this notion, we have observed that PI3K-mutated CRC cells are resistant to BKM120 treatment, which induces a robust increase of autophagy associated to enhanced MEK/ERK signaling.

Previous observations in lung cancer cells showed the ability of BKM120 to induce autophagy with the contribution of similar signaling routes, and the effectiveness of the combination therapy with MEK or autophagy inhibitors [48]. However, the mechanisms underlying the increased autophagic flux were not clarified.

Since PI3K-AKT axis activates mTOR through TSC2 and Rheb, and since mTOR is known to trigger the autophagic flux via ULK1 and AMBRA1, it would be expected that BKM120 treatment induces autophagy simply by preventing mTOR activation. However, in this work we demonstrate that the increase of MYC content, which occurs through FOXO3a-dependent transcriptional activation mediated by its UR, is necessary to induce autophagy and to mediate this mechanism of resistance, as demonstrated in cells lacking MYC UR that do not activate autophagy in response to BKM120.

In a previous work, MYC was shown to be involved in autophagosome formation in the early stages of autophagy [60], while in another report it was shown that MYC occupies the promoter region of key target genes involved in lysosomal biogenesis and autophagy [51]. Consistently, we have observed that the PI3K-mediated induction of autophagy is abrogated in the absence of MYC and that BKM120 induces a MYC-mediated autophagic transcriptional program. Moreover, since the blockade of this compensatory response with autophagy inhibitors successfully abrogates resistance to PI3K inhibitors in relevant in vivo models, these data provide a rationale for the use of the dual blockade of PI3K and autophagy in PI3K-activated colorectal cancers.

It would be important to understand whether PI3K resistance correlates with the loss of exon 1/UR region and/or with MYC upregulation of human CRC patients, by consulting publicly available databases. However, since the use of PI3K inhibitors has not been approved for CRC yet, this analysis is not feasible at the moment, but will most certainly represent an important future goal.

Excitingly, our data unveil that this mechanism may also represent a novel avenue in the treatment of Burkitt Lymphoma, the fastest growing human tumor that accounts for 40% of the yearly diagnosed childhood non-Hodgkin's Lymphoma in the United States of America [61]. While the disease is a highly treatable malignancy, 10% of patients are still resistant to current therapies [62, 63]. The sensitivity of Burkitt Lymphoma cells lacking the MYC UR to PI3K inhibition in a genomic context is novel, and worth further investigation. Here, we have identified a sensitivity to PI3K inhibition in translocation-specific cases of Burkitt Lymphoma. Mechanistically, we found that if the translocated MYC CDS is disjoint from the regulatory MYC UR, the cells cannot induce a MYC-dependent autophagic adaptation in response to PI3K inhibition, and subsequently suffer from a robust antiproliferative response.

Despite BL being a highly treatable disease, children diagnosed as clinically high-risk (risk groups R3 and R4) were found to have relapse rates exceeding 15%, and survival rate at relapse of a mere 20% [64]. In the referenced investigation, authors found that among clinically high-risk children, 44% had translocations within intron 1 or exon 1 of MYC. In another investigation, 62% of pediatric patients with sporadic BL exhibited a translocation within intron 1 or exon 1 of MYC [65]. This could imply that a significant proportion of children with the highest relapse rate of BL and with the lowest survival rates at relapse could potentially benefit from PI3K-targeted chemotherapy. As of now, the use of PI3K inhibitors in a clinical trial of Burkitt Lymphoma has not been attempted. The results presented here would then suggest a potential applicability of PI3K inhibition in the treatment of Burkitt Lymphoma.

MATERIALS AND METHODS

CRISPR/Cas9-mediated deletion of MYC UR

MYC IRES was excised by using short guide RNA (sgRNA) targeting the region 363 to 94 base-pairs upstream the non-canonical CTG start codon [17, 18]. The sequences are described in Supplementary Table II. For transient expression of Cas9 and sgRNAs, HCT116 and SW620 cells were transfected with the constructs and selected with puromycin (#ALX-380-028, Enzo Life Sciences, Farmingdale, NY, USA) for 72 h, then diluted in a 96-well cell plate to allow monoclonal growth, collected, and screened via PCR using the screening primers described in Supplementary Table II. The clones identified as homozygous ΔUR were then subjected to Sanger sequencing.

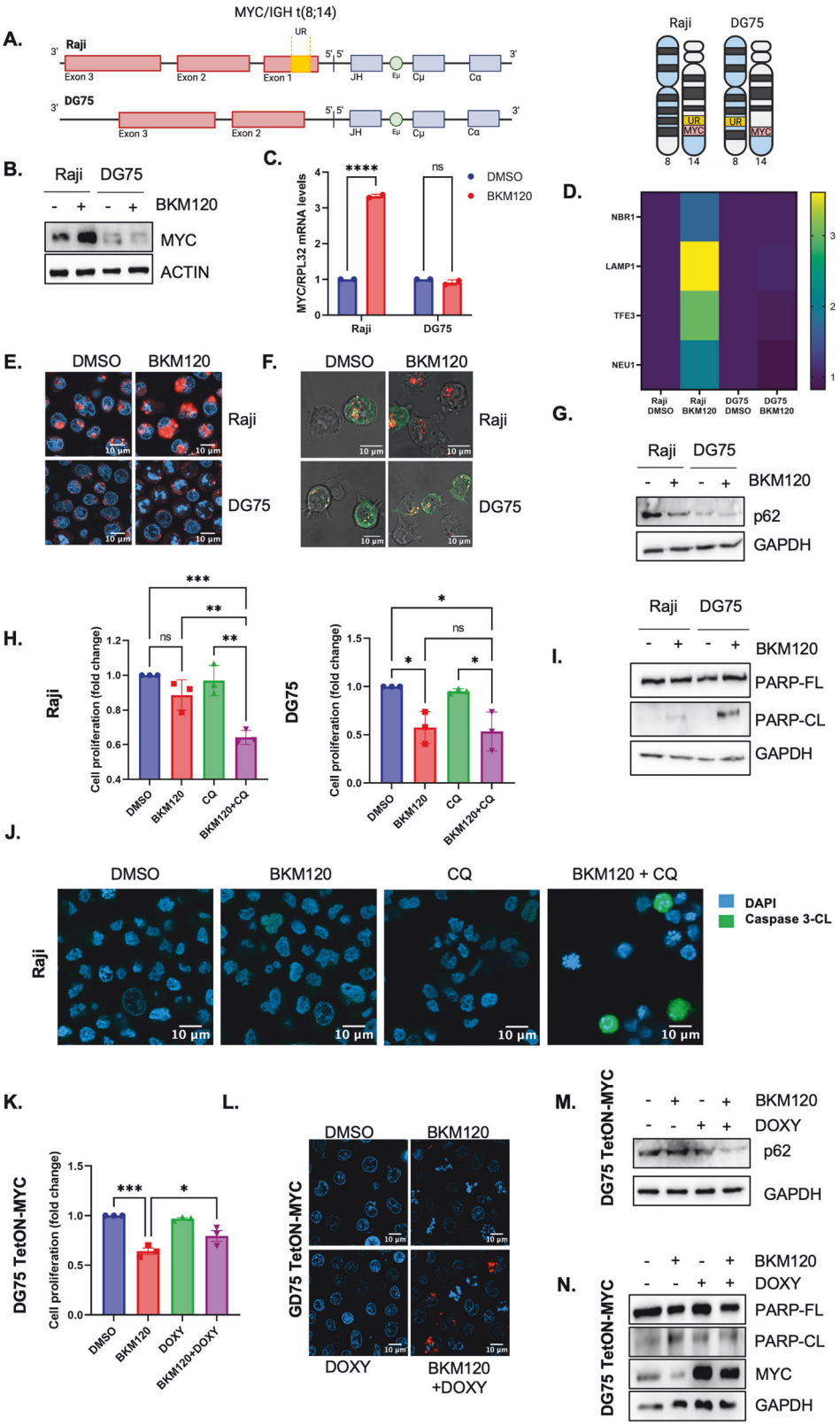

Polysomal fractionation

Polysomal fractionation was performed as previously described [66, 67]. HCT116 and SW620 cells were processed and MYC mRNA distribution in the differing polysomal fractions were analyzed as previously described [68]. Synthetic spike-in RNA was used as a normalization control, with 1 ng added to the pooled fractions immediately before RNA extraction.

Lentivirus-mediated shRNA knockdown and overexpression

Production of lentiviruses was performed as previously described [69]. To perform lentiviral transduction, cells were seeded at a density of $2.0 * 10^4$/cm^2 and transduced with lentiviruses the day after with polybrene (8 μg/mL, #H9268, Sigma-Aldrich, Burlington, MA, USA). Knockdown efficiency was monitored by RT-qPCR. For overexpression of the Tet-ON 4EBP 4XALA,

Fig. 7 Autophagic chemoresistance mediated by the MYC UR is abrogated in translocation-specific Burkitt Lymphoma cells. A Left panel: Schematic of the t(8;14) translocation in Raji and DG75 Burkitt Lymphoma cell lines. Right panel: Schematic demonstrating the juxtaposition of the MYC UR (yellow) and MYC coding sequence (pink) on the t(8; 14) translocated chromosomes in Raji and DG75 cells. Image created in BioRender. **B** Immunoblot showing Raji and DG75 cells treated with 1 μM BKM120 or vehicle (DMSO) for 24 h. **C** QPCR analysis of Raji and DG75 cells treated with 1 μM BKM120 or vehicle (DMSO) for 24 h. RPL32 mRNA levels were used to normalize the data (n = 2). **D** Heatmap of mRNA expression analyzed by QPCR of autophagy-related genes (NBR1, LAMP-1, TFE3, and NEU1) relative to RPL32 in Raji and DG75 cells treated with 1 μM BKM120 or vehicle (DMSO) for 24 h (n = 2). **E** Representative confocal images of Raji and DG75 cells treated with 1 μM BKM120 or vehicle (DMSO) and stained with the fluorescently labeled lysosomal probe Lysotracker Red for 30 min before imaging. DAPI (blue) is a nuclear counterstain. Scale bar 10 μm. **F** Representative confocal images of Raji and DG75 cells transduced with the lentivirus expressing the mCherry-GFP-LC3 and treated with 1 μM BKM120 or vehicle (DMSO) for 24 h. Yellow puncta indicate autophagosomes (mCherry + / GFP +) while autolysosomes appear red (mCherry + /GFP −). Scale bar 10 μm. **G** Immunoblot of Raji and DG75 cells treated with 1 μM BKM120 or vehicle (DMSO) for 24 h. **H** Proliferation assay in Raji (left panel) and DG75 (right panel) cells treated with vehicle (BKM120: DMSO; chloroquine: H_2O), 0.1 μM BKM120, 0.4 nM chloroquine (CQ) or the two drugs in combination (BKM120 + CQ) for 7 days. Data are normalized to DMSO-treated cell number (n = 3). **I** Immunoblot of Raji and DG75 cells treated with 1 μM BKM120 or vehicle (DMSO) for 24 h. **J** Representative confocal images of Raji cells treated for 48 h with vehicle (BKM120: DMSO; CQ: H_2O), 1 μM BKM120, 2 nM CQ or with the two drugs in combination, then subsequently fixed in formaldehyde and stained with anti-cleaved caspase-3 antibody (green) and DAPI (blue) as a nuclear counterstain. Scale bar 10 μm. **K** Proliferation assay in DG75 cells transduced with a MYC doxycycline-inducible lentivirus (DG75 TetON-MYC) then treated with vehicle (BKM120: DMSO; doxycycline: H_2O), 0.1 μM BKM120, 0.1 μg/mL doxycycline, or the two drugs in combination for 7 days. Data are expressed as fold change relative to DMSO-treated cells (n = 3). **L** Representative confocal images of DG75 TetON-MYC cells treated with vehicle (BKM120: DMSO; doxycycline: H_2O), 1 μM BKM120, 0.1 μg/mL doxycycline, or the two drugs in combination and stained with the lysosomal probe Lysotracker Red for 30 min before imaging. DAPI (blue) is a nuclear counterstain. Scale bar 10 μm. **M** Immunoblot of DG75 TetON-MYC treated with vehicle (BKM120: DMSO; doxycycline: H_2O), 1 μM BKM120, 0.1 μg/mL doxycycline, or the two drugs in combination for 24 h. **N** Immunoblot of DG75 TetON-MYC treated with vehicle (BKM120: DMSO; doxycycline: H_2O), 1 μM BKM120, 0.1 μg/mL doxycycline, or the two drugs in combination for 24 h. Data represent the mean ± SD of experiments performed in triplicate. ns = not significant (p > 0.05), *p < 0.05, **p < 0.01, ****p < 0.000,1 by One-way ANOVA followed by post-hoc Tukey's multivariate analysis.

cells infected for 72 h were selected via puromycin (5 μg/mL, #ALX-380-028, Enzo Life Sciences) for 72 h, then treated with 1 μg/mL doxycycline (#D9891, Sigma-Aldrich) for the indicated times.

Xenograft mouse model

Subcutaneous transplantation of tumor cells was performed as previously described [68, 70]. Briefly, 1 * 10^6 cells were resuspended in 50 μL PBS solution, mixed with equal volume of Matrigel (#354248, Corning, Corning, NY, USA) and implanted subcutaneously in both flanks of 8-week-old female CD1 athymic nude mice (Charles River Laboratories, Wilmington, MA, USA). When the tumor volumes reached 100 mm^3, mice were randomly assigned to different treatment groups, administered daily by oral gavage for 15 days with 30 mg/kg BKM120 suspended in a mixture of 90% corn oil and 10% DMSO or the vehicle alone. For the xenograft of patient-derived Colorectal Cancer stem cells, the animals underwent the same procedure and administered daily by oral gavage with 30 mg/kg BKM120 suspended in a mixture of 90% corn oil and 10% DMSO or the vehicle alone, and an intraperitoneal injection of 30 mg/kg chloroquine in 0.9% normal saline, or vehicle alone, for 12 days. Animals were excluded if their health status did not comply with health regulations. Tumor volume was monitored every 3 days using a caliper and calculated as $V = (L \times W^2)/2$. Growth patterns were summarized graphically by plotting the mean and SD for each group over time. Investigators were blind to the treatment groups for ex-vivo analyses. For in vivo experiments, the number of animals per group was established using the G-power calculation to guarantee a statistical power of 80% (alpha error <0.05) for pairwise mean differences of at least 1.5 standard deviations (effect size).

Animal studies were performed according to the European Community Council Directive 2010/63/EU. The study was carried out under the approval of the Institutional Animal Care Committee and by the Ministry of Health.

Intestinal tumor organoids

Intestinal tumor organoids were established as described [71]. Briefly, small intestine was explanted from a 17-week-old male $APC^{Min+/-}$ mouse and tumors were isolated using a dissecting microscope. Tumors were incubated in EDTA chelation buffer for 60 min on ice, then digested in 200 U/mL type IV collagenase and 125 μg/mL type II dispase. Single cells were suspended in 5 mg/mL Matrigel and cultured in basal culture medium (100 μg/mL Primocin (#ant-pm-05, InvivoGen, San Diego, CA, USA), 10 mmol/L HEPES, 2 mM Glutamax, 1xN2 supplement, 1xB27 supplement, 1 mmol/L N-acetylcysteine in Advanced Dulbecco's Modified Eagle Medium/F12) containing 50 ng/mL murine EGF. Treatments were added at the indicated concentrations to the basal culture medium after seeding and pictures were taken after 48 or 72 h. Tumoroids diameter was measured using ImageJ 1.54 f software.

DATA AVAILABILITY

All data generated during and/or analyzed during the current study are available from the corresponding author on reasonable request.

REFERENCES

1. Dang CV, O'Donnell KA, Zeller KI, Nguyen T, Osthus RC, Li F. The c-Myc target gene network. Semin Cancer Biol. 2006;16:253–64.
2. ar-Rushdi A, Nishikura K, Erikson J, Watt R, Rovera G, Croce CM. Differential expression of the translocated and the untranslocated c-myc oncogene in Burkitt lymphoma. Science. 1983;222:390–3.
3. Dalla-Favera R, Bregni M, Erikson J, Patterson D, Gallo RC, Croce CM. Human c-myc onc gene is located on the region of chromosome 8 that is translocated in Burkitt lymphoma cells. Proc Natl Acad Sci USA. 1982;79:7824–7.
4. Taub R, Kirsch I, Morton C, Lenoir G, Swan D, Tronick S, et al. Translocation of the c-myc gene into the immunoglobulin heavy chain locus in human Burkitt lymphoma and murine plasmacytoma cells. Proc Natl Acad Sci USA. 1982;79:7837–41.
5. Rabbitts TH, Hamlyn PH, Baer R. Altered nucleotide sequences of a translocated c-myc gene in Burkitt lymphoma. Nature. 1983;306:760–5.
6. Pelengaris S, Khan M, Evan G. c-MYC: more than just a matter of life and death. Nat Rev Cancer. 2002;2:764–76.
7. Lee KS, Kwak Y, Nam KH, Kim DW, Kang SB, Choe G, et al. c-MYC copy-number gain is an independent prognostic factor in patients with colorectal cancer. PLoS One. 2015;10:e0139727.
8. Kakisako K, Miyahara M, Uchino S, Adachi Y, Kitano S. Prognostic significance of c-myc mRNA expression assessed by semi-quantitative RT-PCR in patients with colorectal cancer. Oncol Rep. 1998;5:441–5.
9. Bhatavdekar JM, Patel DD, Ghosh N, Chikhlikar PR, Trivedi TI, Suthar TP, et al. Coexpression of Bcl-2, c-Myc, and p53 oncoproteins as prognostic discriminants in patients with colorectal carcinoma. Dis Colon Rectum. 1997;40:785–90.
10. Rowley S, Newbold KM, Gearty J, Keighley MR, Donovan IA, Neoptolemos JP. Comparison of deoxyribonucleic acid ploidy and nuclear expressed p62 c-myc oncogene in the prognosis of colorectal cancer. World J Surg. 1990;14:545–50. discussion 551
11. Wang C, Zhang J, Yin J, Gan Y, Xu S, Gu Y, et al. Alternative approaches to target Myc for cancer treatment. Sig Transduct Target Ther. 2021;6:1–14.
12. Struntz NB, Chen A, Deutzmann A, Wilson RM, Stefan E, Evans HL, et al. Stabilization of the max homodimer with a small molecule attenuates Myc-driven transcription. Cell Chem Biol. 2019;26:711–23.e14.

13. Llombart V, Mansour MR. Therapeutic targeting of "undruggable" MYC. EBioMedicine 2021;75:103756.
14. Whitfield JR, Beaulieu ME, Soucek L. Strategies to inhibit Myc and their clinical applicability. Front Cell Dev Biol [Internet]. 2017;5. [cited 2024 Feb 17]. Available from: https://www.frontiersin.org/articles/10.3389/fcell.2017.00010
15. De Benedetti A, Graff JR. eIF-4E expression and its role in malignancies and metastases. Oncogene. 2004;23:3189–99.
16. Shi Y, Sharma A, Wu H, Lichtenstein A, Gera J. Cyclin D1 and c-myc internal ribosome entry site (IRES)-dependent translation is regulated by AKT activity and enhanced by rapamycin through a p38 MAPK- and ERK-dependent pathway*. J Biol Chem. 2005;280:10964–73.
17. Nanbru C, Lafon I, Audigier S, Gensac MC, Vagner S, Huez G, et al. Alternative translation of the proto-oncogene c-myc by an internal ribosome entry site. J Biol Chem. 1997;272:32061–6.
18. Stoneley M, Paulin FE, Quesne JPL, Chappell SA, Willis AE. C-Myc 5′ untranslated region contains an internal ribosome entry segment. Oncogene. 1998;16:423–8.
19. Walsh D, Mathews MB, Mohr I. Tinkering with translation: protein synthesis in virus-infected cells. Cold Spring Harb Perspect Biol. 2013;5:a012351.
20. Pelletier J, Sonenberg N. Internal initiation of translation of eukaryotic mRNA directed by a sequence derived from poliovirus RNA. Nature. 1988;334:320–5.
21. Jang SK, Kräusslich HG, Nicklin MJ, Duke GM, Palmenberg AC, Wimmer E. A segment of the 5′ nontranslated region of encephalomyocarditis virus RNA directs internal entry of ribosomes during in vitro translation. J Virol. 1988;62:2636–43.
22. Komar AA, Hatzoglou M. Cellular IRES-mediated translation. Cell Cycle. 2011;10:229–40.
23. Subkhankulova T, Mitchell SA, Willis AE. Internal ribosome entry segment-mediated initiation of c-Myc protein synthesis following genotoxic stress. Biochem J. 2001;359:183–92.
24. Stoneley M, Chappell SA, Jopling CL, Dickens M, MacFarlane M, Willis AE. c-Myc protein synthesis is initiated from the internal ribosome entry segment during apoptosis. Mol Cell Biol. 2000;20:1162–9.
25. Yeh DW, Zhao X, Siddique HR, Zheng M, Choi HY, Machida T, et al. MSI2 promotes translation of multiple IRES-containing oncogenes and virus to induce self-renewal of tumor initiating stem-like cells. Cell Death Discov. 2023;9:1–15.
26. Grentzmann G, Ingram JA, Kelly PJ, Gesteland RF, Atkins JF. A dual-luciferase reporter system for studying recoding signals. RNA. 1998;4:479–86.
27. Kozak M. New Ways of Initiating Translation in Eukaryotes? Mol Cell Biol. 2001;21:1899–907.
28. Hellen CUT, Sarnow P. Internal ribosome entry sites in eukaryotic mRNA molecules. Genes Dev. 2001;15:1593–612.
29. Bert AG, Grépin R, Vadas MA, Goodall GJ. Assessing IRES activity in the HIF-1α and other cellular 5′ UTRs. RNA. 2006;12:1074–83.
30. Baranick BT, Lemp NA, Nagashima J, Hiraoka K, Kasahara N, Logg CR. Splicing mediates the activity of four putative cellular internal ribosome entry sites. Proc Natl Acad Sci USA. 2008;105:4733–8.
31. Wang Z, Weaver M, Magnuson NS. Cryptic promoter activity in the DNA sequence corresponding to the pim-1 5′-UTR. Nucleic Acids Res. 2005;33:2248–58.
32. Van Eden ME, Byrd MP, Sherrill KW, Lloyd RE. Demonstrating internal ribosome entry sites in eukaryotic mRNAs using stringent RNA test procedures. RNA. 2004;10:720–30.
33. Shi Y, Yang Y, Hoang B, Bardeleben C, Holmes B, Gera J, et al. Therapeutic potential of targeting IRES-dependent c-myc translation in multiple myeloma cells during ER stress. Oncogene. 2016;35:1015–24.
34. Denk S, Schmidt S, Schurr Y, Schwarz G, Schote F, Diefenbacher M, et al. CIP2A regulates MYC translation (via its 5′UTR) in colorectal cancer. Int J Colorectal Dis. 2021;36:911–8.
35. Martinez-Useros J, Garcia-Carbonero N, Li W, Fernandez-Aceñero MJ, Cristobal I, Rincon R, et al. UNR/CSDE1 expression is critical to maintain invasive phenotype of colorectal cancer through regulation of c-MYC and epithelial-to-mesenchymal transition. J Clin Med. 2019;8:560.
36. Spriggs KA, Cobbold LC, Jopling CL, Cooper RE, Wilson LA, Stoneley M, et al. Canonical initiation factor requirements of the myc family of internal ribosome entry segments. Mol Cell Biol. 2009;29:1565–74.
37. Wiegering A, Uthe FW, Jamieson T, Ruoss Y, Hüttenrauch M, Küspert M, et al. Targeting translation initiation bypasses signaling crosstalk mechanisms that maintain high MYC levels in colorectal cancer. Cancer Discov. 2015;5:768–81.
38. Thoreen CC, Chantranupong L, Keys HR, Wang T, Gray NS, Sabatini DM. A unifying model for mTORC1-mediated regulation of mRNA translation. Nature. 2012;485:109–13.
39. Pyronnet S, Pradayrol L, Sonenberg N. A cell cycle-dependent internal ribosome entry site. Mol Cell. 2000;5:607–16.
40. Shi Y, Sun F, Cheng Y, Holmes B, Dhakal B, Gera JF, et al. Critical role for cap-independent c-MYC translation in progression of multiple myeloma. Mol Cancer Therapeutics. 2022;21:502–10.
41. Karar J, Cerniglia GJ, Lindsten T, Koumenis C, Maity A. Dual PI3K/mTOR inhibitor NVP-BEZ235 suppresses hypoxia-inducible factor (HIF)-1α expression by blocking protein translation and increases cell death under hypoxia. Cancer Biol Ther. 2012;13:1102–11.
42. Burger MT, Pecchi S, Wagman A, Ni ZJ, Knapp M, Hendrickson T, et al. Identification of NVP-BKM120 as a potent, selective, orally bioavailable class I PI3 kinase inhibitor for treating cancer. ACS Med Chem Lett. 2011;2:774–9.
43. Ilic N, Utermark T, Widlund HR, Roberts TM. PI3K-targeted therapy can be evaded by gene amplification along the MYC-eukaryotic translation initiation factor 4E (eIF4E) axis. Proc Natl Acad Sci USA. 2011;108:E699–708.
44. Wright CJM, McCormack PL. Trametinib: first global approval. Drugs. 2013;73:1245–54.
45. Liu J, Long S, Wang H, Liu N, Zhang C, Zhang L, et al. Blocking AMPK/ULK1-dependent autophagy promoted apoptosis and suppressed colon cancer growth. Cancer Cell Int. 2019;19:336.
46. Degenhardt K, Mathew R, Beaudoin B, Bray K, Anderson D, Chen G, et al. Autophagy promotes tumor cell survival and restricts necrosis, inflammation, and tumorigenesis. Cancer Cell. 2006;10:51–64.
47. Yang W, Hosford SR, Traphagen NA, Shee K, Demidenko E, Liu S, et al. Autophagy promotes escape from phosphatidylinositol 3-kinase inhibition in estrogen receptor–positive breast cancer. FASEB J. 2018;32:1222–35.
48. Ren H, Guo H, Thakur A, Zhang S, Wang T, Liang Y, et al. Blockade efficacy of MEK/ERK-dependent autophagy enhances PI3K/Akt inhibitor NVP-BKM120's therapeutic effectiveness in lung cancer cells. Oncotarget. 2016;7:67277–87.
49. Pankiv S, Clausen TH, Lamark T, Brech A, Bruun JA, Outzen H, et al. p62/SQSTM1 binds directly to Atg8/LC3 to facilitate degradation of ubiquitinated protein aggregates by autophagy *. J Biol Chem. 2007;282:24131–45.
50. Bjørkøy G, Lamark T, Pankiv S, Øvervatn A, Brech A, Johansen T. Monitoring autophagic degradation of p62/SQSTM1. Methods Enzymol. 2009;452:181–97.
51. Annunziata I, van de Vlekkert D, Wolf E, Finkelstein D, Neale G, Machado E, et al. MYC competes with MiT/TFE in regulating lysosomal biogenesis and autophagy through an epigenetic rheostat. Nat Commun. 2019;10:3623.
52. Mangiapane LR, Nicotra A, Turdo A, Gaggianesi M, Bianca P, Di Franco S, et al. PI3K-driven HER2 expression is a potential therapeutic target in colorectal cancer stem cells. Gut. 2022;71:119–28.
53. López C, Burkhardt B, Chan JKC, Leoncini L, Mbulaiteye SM, Ogwang MD, et al. Burkitt lymphoma. Nat Rev Dis Prim. 2022;8:1–26.
54. Shiramizu B, Magrath I. Localization of breakpoints by polymerase chain reactions in Burkitt's lymphoma with 8;14 translocations. Blood. 1990;75:1848–52.
55. Basso K, Frascella E, Zanesco L, Rosolen A. Improved long-distance polymerase chain reaction for the detection of t(8;14)(q24;q32) in Burkitt's lymphomas. Am J Pathol. 1999;155:1479–85.
56. Papadatos-Pastos D, Rabbie R, Ross P, Sarker D. The role of the PI3K pathway in colorectal cancer. Crit Rev Oncol Hematol. 2015;94:18–30.
57. Zhu M, Jin Q, Xin Y. Recent clinical advances in PI3K inhibitors on colorectal cancer. Pharmazie 2021;76:568–73.
58. Mele L, Del Vecchio V, Liccardo D, Prisco C, Schwerdtfeger M, Robinson N, et al. The role of autophagy in resistance to targeted therapies. Cancer Treat Rev. 2020;88:102043.
59. Chang H, Zou Z. Targeting autophagy to overcome drug resistance: further developments. J Hematol Oncol. 2020;13:159.
60. Toh PPC, Luo S, Menzies FM, Raskó T, Wanker EE, Rubinsztein DC. Myc inhibition impairs autophagosome formation. Hum Mol Genet. 2013;22:5237–48.
61. Swerdlow SH, Campo E, Harris NL, Jaffe ES, Pileri SA, Stein H, et al. WHO classification of tumours of haematopoietic and lymphoid tissues. Revised 4th edition. Lyon: International Agency for Research on Cancer; 2017. 585 p. (World Health Organization classification of tumours).
62. Kim H, Park ES, Lee SH, Koo HH, Kim HS, Lyu CJ, et al. Clinical outcome of relapsed or refractory burkitt lymphoma and mature B-cell lymphoblastic leukemia in children and adolescents. Cancer Res Treat. 2014;46:358–65.
63. Patte C, Auperin A, Michon J, Behrendt H, Leverger G, Frappaz D, et al. The Société Française d'Oncologie Pédiatrique LMB89 protocol: highly effective multiagent chemotherapy tailored to the tumor burden and initial response in 561 unselected children with B-cell lymphomas and L3 leukemia. Blood. 2001;97:3370–9.
64. Möker P, zur Stadt U, Zimmermann M, Alawi M, Mueller S, Finger J, et al. Characterization of IG-MYC-breakpoints and their application for quantitative minimal disease monitoring in high-risk pediatric Burkitt-lymphoma and. Leukemia. 2022;36:2343–6.
65. Busch K, Keller T, Fuchs U, Yeh RF, Harbott J, Klose I, et al. Identification of two distinct MYC breakpoint clusters and their association with various IGH breakpoint regions in the t(8;14) translocations in sporadic Burkitt-lymphoma. Leukemia. 2007;21:1739–51.

66. Coni S, Serrao SM, Yurtsever ZN, Di Magno L, Bordone R, Bertani C, et al. Blockade of EIF5A hypusination limits colorectal cancer growth by inhibiting MYC elongation. Cell Death Dis. 2020;11:1–14.
67. Coni S, Falconio FA, Marzullo M, Munafò M, Zuliani B, Mosti F, et al. Translational control of polyamine metabolism by CNBP is required for Drosophila locomotor function. Ramaswami M, VijayRaghavan K, Ramaswami M, editors. eLife. 2021;10:e69269.
68. Coni S, Bordone R, Ivy DM, Yurtsever ZN, Di Magno L, D'Amico R, et al. Combined inhibition of polyamine metabolism and eIF5A hypusination suppresses colorectal cancer growth through a converging effect on MYC translation. Cancer Lett. 2023;559:216120.
69. D'Amico D, Antonucci L, Di Magno L, Coni S, Sdruscia G, Macone A, et al. Non-canonical Hedgehog/AMPK-mediated control of polyamine metabolism supports neuronal and medulloblastoma cell growth. Dev Cell. 2015;35:21–35.
70. Di Magno L, Manni S, Di Pastena F, Coni S, Macone A, Cairoli S, et al. Phenformin Inhibits Hedgehog-dependent tumor growth through a complex I-independent redox/corepressor module. Cell Rep. 2020;30:1735–1752.e7.
71. Xue X, Shah YM. In vitro organoid culture of primary mouse colon tumors. JoVE (J Visualized Exp). 2013;75:e50210.

ACKNOWLEDGEMENTS

We thank Drs Pankaj Trivedi and Eleni Anastasiadou for sharing Raji and DG75 cells and advice, and Drs Cristiano Simone and Martina Lepore Signorile for providing FOXO3a expression vector and antibody. This work was funded by the Fondazione AIRC (Associazione Italiana per la Ricerca sul Cancro) IG 25833 to GC, IG20801 to LuDM, IG24329 to GG, AIRC Italy Post-Doc fellowship (to RB), MIUR PRIN 2022 2022L332YR (GC), MIUR PRIN 2022 under 40 2022J8X7PJ (SC) Sapienza University of Rome RG12117A61923A6F (GC), Institute Pasteur Italy—Fondazione Cenci Bolognetti, call 2020 "Anna Tramontano" (GC), Fondazione Umberto Veronesi fellowship (to LDM), Dipartimenti di Eccellenza 2018-2022 and 2023-2027 (L. 232/2016).

AUTHOR CONTRIBUTIONS

GC conceived and coordinated the project, designed experiments, analyzed data and wrote the paper, RB and DMI designed and performed experiments, analyzed data, and wrote the paper, RDA, MB, FDP, BC, FB, AB, MG performed experiments and analyzed data, EDS, GG, LuDM, AF, LDM, SC, GS analyzed data and reviewed the manuscript.

COMPETING INTERESTS

The authors declare no competing interests.

ETHICS APPROVAL AND CONSENT TO PARTICIPATE

All methods involving human derived materials and animal subjects were performed in accordance with the relevant local regulation and guidelines. All mouse experiments were performed according to the European Community Council Directive 2010/63/EU and carried out under the approval of the Institutional Animal Care Committee and Ministry of Health (protocol n. C1368.26). Patient-derived colorectal cancer stem cells were obtained in accordance with the ethical standards regarding Human Experimentation and informed consent was obtained from each patient in this study under Institutional Review Board protocols (authorization CE9/2015, Policlinico Paolo Giaccone, Palermo, Italy).

ADDITIONAL INFORMATION

Supplementary information The online version contains supplementary material available at https://doi.org/10.1038/s41388-024-03170-6.

Correspondence and requests for materials should be addressed to Gianluca Canettieri.